

BRITISH GEOLOGICAL SURVEY
TECHNICAL REPORT WM/89/19
Geomagnetism Series

TECHNICAL REPORT WM/89/19

TECHNICAL REPORT WM/89/19

**AN INTERPRETATION OF DEEP GEOELECTRIC
RESULTS ACROSS A HOT DRY ROCK GRANITE**

David Beamish

Subject index

Geoelectric, geothermal, hot dry rock,
granite.

Bibliographic reference

Beamish, D., An interpretation of deep
geoelectric results across a Hot Dry
Rock granite. British Geological Survey,
Technical Report, WM/89/15.

This report has been generated from a scanned image of the document with any blank pages removed at the scanning stage.
Please be aware that the pagination and scales of diagrams or maps in the resulting report may not appear as in the original

CONTENTS

1 INTRODUCTION

2 THE FIELD SURVEY

3 RESULTS OF THE SURVEY

Dimensionality indicators

Anisotropy ratios

Rotational characteristics

4 THE VERTICAL RESISTIVITY PROFILE

5 BACKGROUND TO THE INTERPRETATION OF RESULTS

The temperature dependence of resistivity

The pressure dependence of resistivity

6 INTERPRETATION OF LATERAL GEOELECTRIC ANISOTROPY

7 INTERPRETATION OF THE VERTICAL CRUSTAL SECTION

8 SUMMARY

ACKNOWLEDGEMENTS

REFERENCES

1 INTRODUCTION

This report considers the results of a field audiomagnetotelluric (AMT) survey carried out across the Carnmenellis granite in SW England. The Carnmenellis granite (CG in the location map of Figure 1) is one of a series of outcropping plutons that occur within the late Carboniferous (Variscan) orogenic belt of Cornwall and Devon. Together the granite plutons make up the Cornubian batholith of SW England. The ridge of granite extends to mid-crustal depths and is some 200 km in length. A development site for the extraction of Hot Dry Rock (HDR) geothermal energy is located on the Carnmenellis granite (Rosemanowes quarry, RQ in Figure 1).

The geotechnical requirements of HDR exploitation (e.g. Batchelor 1984) require assessments of rock/fluid properties down to depths of at least 6 km where temperatures are predicted to be in excess of 200 °C (Anon 1987). This depth range is immediately accessible using the frequency bandwidth of present-day AMT sounding equipment. Results relating to the upper 10 km of the crustal section are presented here.

Each sounding represents an approximately hemispherical volume of electromagnetic wave propagation beneath and around the site. The radius comprises both depth and lateral distance. Since it is a *volume* sounding (at a point), the fields and results may be influenced and interpreted in a full 3-dimensional (3-D) sense. For simplicity, and usually because of insufficient density of observations, the methods of interpretation attempt to separate results related to 1-dimensionality (the vertical resistivity profile) from the 2-dimensional azimuthal information related to geoelectric anisotropy.

Established compilations of representative resistivity values of crystalline, and in particular granitic, rocks suggest very high values in excess of 10,000 ohm.m (e.g. Telford *et al.* 1976). While such values may be representative of 'intact' crystalline rock they are not in accord with the results of the present survey which provides values of 1,000 to 10,000 ohm.m for the upper crustal section. In such circumstances the Carnmenellis granite must be viewed as comprising very resistive 'intact' rock and many voids such as joints, cracks and pores which are saturated with interstitial fluids. Both the flow of fluid (governed by the permeability of the rock) and the flow of electric current (governed by the resistivity of the rock) are then principally controlled by the nature of the void and fluid content (Walsh and Brace 1984). The applicability of such a model appears to be confirmed by an examination of the resistivity laterologs from the geothermal wells at Rosemanowes quarry (supplied by the Camborne School of Mines). The deepest well (RH15), logged to a depth of 2.8 km, reveals intact formation resistivities of the order of the tool limit (200,000 ohm.m) but with a considerable depth-integrated density of fracture resistivities descending to several thousand, and in some cases, to several hundred ohm.m. The bulk resistivity in such circumstances will be controlled by the low resistivity fluid content of fractures and pores within the resistive intact matrix.

Granite-water interactions in the Carnmenellis granite have been considered by Burgess *et al.* (1982) and by Edmunds *et al.* (1988). Mining operations in Cornwall have encountered high salinity groundwaters within the granite and adjacent rocks. These waters have a salinity of up to 30 g.l⁻¹. The present thermal waters (up to 55 °C) probably represent active circulation cells (down to about 1.1 km) composed of recent descending meteoric waters and older saline water circulating very slowly in the granite. The results imply that fracture permeability is an important feature of the granite. It is considered likely that the natural groundwater at depths of 6-7 km will have a salinity in excess of 30 g.l⁻¹ (Edmunds *et al.* 1988).

The regional geometry of the batholith has been examined by gravity modelling (Willis-Richards 1986; Sams and Thomas-Betts 1988). These studies, combined with a few conclusions that can be drawn from seismic experiments, support the idea of the granite being homogeneous down to a flat base. The base of the granite has been estimated as between 10 and 15 km from seismic refraction studies (Brooks *et al.* 1984) and at 13 km from 3-D gravity modelling (Willis-Richards 1986). The wide-angle seismic refraction results of Brooks *et al.* (1984) suggest an acoustic interface (R1) in the depth range 7 to 8 km. Survey line 4 crossing the Carnmenellis granite observed two reflectors (R1,R2) above the Moho. The shallow reflector (R1) appeared to be confined to the granite. The model reflector R1 defines the upper surface of a low velocity zone which extends to the second reflector (R2) in the depth interval 12 to 15 km.

Two further influences on the electrical properties of granite that must be considered are temperature and pressure. The Cornubian batholith is characterised by the highest measured heat flow values in the UK. The heat flow field and subsurface temperatures for the Carnmenellis granite are discussed by Wheildon and Rollin (1986), Lee (1986) and by Sams and Thomas-Betts (1988). The predicted sub-surface temperature profile for the Carnmenellis granite, calculated from a 1-D heat transfer model, is shown in Figure 2. The profile depends on the assumed depth dependence of heat production and thermal conductivity. The profile shown uses the parameters adopted by Wheildon and Rollin (1986) and Lee (1986). The model predicts a temperature of 200 °C at about 5.4 km and indicates a temperature of 370 °C at a depth of 10 km.

For a realistic granite mass, and the Carnmenellis granite in particular, the pressure dependence should take into account the likely influence of both the jointed nature of the granite and the in-situ, highly deviatoric stress distribution. The joint/fracture types of the Carnmenellis granite have been discussed by a number of authors. According to Heath (1985), two groups of joints are observed at the surface. The directions of the two principal *surface* joint sets are shown (shaded) in Figure 3 (after Batchelor 1984; Green *et al.* 1987). A further feature of the Carnmenellis granite is the anisotropic nature of the horizontal stress field at depth (Green *et al.* 1987). Also shown in Figure 3 are the directions and magnitudes of the maximum and minimum horizontal stresses at a depth of 2 km. The vertical (overburden) stress is intermediate between these two extremes. The influence of pressure/stress and temperature effects are discussed in more detail following a description of the field survey and the results obtained.

2 THE FIELD SURVEY

The audiomagnetotelluric (AMT) survey was undertaken in 1988 using an in-house AMT field system. The computer-based system collects and analyses 7 channels of natural electromagnetic fields across a frequency range from 100 to 0.01 Hz. The system provides a composite bandwidth using four decade ranges. The seven channels of data are two local electric fields, three local magnetic fields and two reference magnetic fields. The two reference magnetic sensors were used in a local reference mode and this proved satisfactory. The approximate separation between local and remote sensors was 200 m. The main sources of noise were localised ground-coupled electric field transients derived from agricultural electric fences. True remote reference operation would not have been advantageous in the circumstances encountered.

The methods of in-field data processing are not described here. The main elements of frequency-domain tensor estimation are based on the established procedures of remote-reference techniques described by Gamble *et al.* (1979) and by Travassos and Beamish (1988).

Figure 1 shows the sounding locations in relation to the outcrop of the Carnmenellis granite. The main E-W profile (solid dots) consisted of 12 sites at a spacing of approximately 1 km. The site numbers of the profile sites are denoted as 101 (western-most) through to 112 (eastern-most) and increase easterly. This set of locations, forming an approximately E-W profile confined to the granite outcrop, will be referred to as SET 1. Site 108 did not provide results of sufficient quality to be included in the present analysis. The results presented are based on the remaining 11 sounding locations.

Two soundings (sites 201 and 202, Figure 1) were obtained off the outcrop primarily for dimensional control and these will be referred to as SET 2 locations. Three further soundings were undertaken in the vicinity of the present geothermal reservoir at Rosemanowes quarry. The results obtained at these SET 3 sounding locations are not discussed here since two of the locations are influenced by the artificial permeability of the geothermal reservoir (Beamish and Riddick 1989). Grid coordinates for the SET 1 and SET 2 sounding locations are provided in Table 1.

3 RESULTS OF THE SURVEY

Because of the 3-D nature of the sounding technique this section attempts to separate results related to one-dimensionality (the vertical resistivity profile) from the two-dimensional azimuthal information related to lateral geoelectric anisotropy. To assist in the interpretation of results frequency has been transformed to an equivalent one-dimensional depth as described below.

Each sounding represents an approximately hemispherical volume of electromagnetic wave propagation beneath and around the site. The radius comprises both depth and lateral distance. Since it is a *volume* sounding, the fields and results may be influenced and interpreted in a full three-dimensional (3-D) sense. The penetration radius increases from a minimum at the highest frequency to a maximum at the lowest frequency used. The actual values achieved depend on the resistivity structure encountered. The sounding values (the impedance tensor as a function of frequency) can be viewed as a 1-D sounding curve which may be perturbed by lateral variations in geoelectric structure. In the near-field of strong lateral contrasts, the lateral effect may well dominate and the concept of a vertical sounding radius is misleading.

Normally magnetotelluric interpretation parameters, derived from the impedance tensor, are plotted as a function of frequency. To assist in the interpretation of results frequency has been transformed to an equivalent depth scale. When the structure encountered is 1-D, it is possible to transform an observed impedance/frequency estimate to an equivalent resistivity(ρ^*)/depth(z^*) estimate. This is the $\rho^* - z^*$ transformation described in detail by Schmucker (1987). Thus in the 1-D case we can map any interpretation parameter from the frequency to the depth (z^*) domain.

When the structure is not 1-D we can usefully employ a rotationally invariant average impedance, derived from the principal (off-diagonal) impedances (Z_{xy} and Z_{yx}) as

$$Z_a = (Z_{xy} - Z_{yx}) / 2$$

Since Z_a is rotationally invariant we can effectively use this impedance to again transform from frequency to depth. The sequence used here in presenting results as a function of depth is to form Z_a at each frequency estimate. This impedance is then transformed to the complex impedance of Weidelt (1972) as

$$c(\omega) = g(\omega) - i.h(\omega) = Z_a(\omega)/i\omega\mu_0$$

Where ω is angular frequency and μ_0 is the magnetic permeability of free space. We then form a depth estimate as

$$z^*(\omega) = \text{Re}(c(\omega)) = g(\omega)$$

with z^* expressed in metres. The estimate is an indicator of the depth in the same sense as a 'centre-of-mass'. The depth z^* is referred to here as a penetration depth.

Penetration depths, defined in this way, provide minimum values at the highest frequencies of the sounding bandwidth. Minimum penetration depths obtained by the survey range from 452 m at site 201 (off the outcrop) to 1.6 km at site 110. Maximum penetration depths at the lowest frequencies exceed 50 km. The properties of the upper 6 km are of most immediate concern to the commercial exploitation of geothermal energy in the Carnmenellis granite. The results

presented here refer to the first 10 km of the crustal section.

Dimensionality indicators

In order to provide reasonable interpretations of the data an assessment of the likely 'dimensional' influences on the sounding curves is first performed. A background to this aspect of interpretation is given by Beamish (1986). The assessment is not exact; it is more a matter of degree.

The skew values (logarithmic scale) for the two sets of site groupings are shown in Figure 4. We are not interested here in the depth dependence since skew is usually an erratic (low signal-to-noise) parameter. The overall magnitude of skew can be used to identify likely 3-D contributions to a sounding curve. For these data we can identify skew values of < 0.2 as 1-D and/or 2-D contributions and skew values > 0.2 as the onset of 3-D contributions. The results of Figure 4 indicate that the off-granite site 202 is the only site to be influenced by a significant 3-D contribution. The grouping of skew values of > 0.1 at large penetration depths for the SET 1 results derive from the eastern-most profile sites 110, 111 and 112.

To further identify dimensional influences, the dimensional weights D1, D2 and D3 (see Beamish 1986) are shown in Figure 5a (SET 1 results) and 5b (SET 2 results). These weights, in the range 0 to 1, attempt to simultaneously assess the *relative* dimensional contributions to the sounding curves. The 1-D (D1) weights shown in Figure 5a are high (> 0.75) for the SET 1 granite sites. The D1 weights display a slight decrease with increasing penetration radius. The 2-D (D2) weights at the SET 1 locations are of the order of 0.1 and are consistent across the granite. The D1 weight at site 201 (Fig. 5b) is clearly low while the D2 (2-D) weight at this site is distinctly high thus confirming strong 2-D contributions at this off-granite site. The D3 weight for site 202 confirms the high skew value at this site and emphasises the 3-D influence at this off-granite site. The dimensional results indicate that for the upper 10 km of the crustal section, the sounding data on the granite possess a strong 1-D contribution while retaining an additional constant and persistent 2-D factor. The degree of 'one-dimensionality' appears to decrease slightly with depth.

Anisotropy ratios

If all the sounding data were 1-D then there would be only vertical (depth) information to be assessed. Since we have established that there exist 2-D influences on the sounding data, rotational characteristics of the impedance tensors can be examined. Conventional methods exist to extract this information based on simple rotations in the horizontal plane (Word *et al.* 1970). More recent and reliable formulations decompose the impedance tensor via an eigenstate analysis thus providing state eigenvalues and eigenvectors (Eggers 1982). The characteristic state formulation of the impedance tensor developed by Tzani (1987) is used here. This analysis provides extremal values (magnitudes, phases and azimuths) of the impedance tensor. From this

analysis the maximum (and minimum) states of the E and H fields can be obtained. The horizontal azimuth of the maximum E state defines a direction of maximum resistivity. The direction of minimum resistivity (maximum H state) will be approximately orthogonal to the direction of maximum resistivity.

Before discussing azimuthal information, the anisotropy ratios defined by the maximum and minimum states are first presented. The anisotropy ratio (AR) is simply defined as the ratio of maximum to minimum apparent resistivities determined by the eigenvalues of the impedance tensor. The lower bound of the AR is of course unity. The results obtained at both SET 1 and SET 2 locations are shown in Figure 6. With the exception of the initial behaviour at site 109, the results for the SET 1 sites are remarkably consistent and form a set of values in the range 1.5 to 3. The AR values at site 201 (strong 2-D) are clearly unique to this site and the rapid movements suggests the near-field influence of strong anisotropy.

Rotational characteristics

The above analysis provides the maximum (and minimum) states of the E and H fields. The horizontal azimuth of the maximum E state, here referred to as GE, defines a direction of *maximum* resistivity. The direction of minimum resistivity will be approximately orthogonal to GE. In simple terms, if the major fluid-filled lineaments of the granite were directed NW-SE then the direction of maximum resistivity (GE) would be NE-SW. We again concentrate on the results from the upper crustal section. All horizontal azimuths refer to grid north and GE is defined in the range $-90^\circ \leq GE \leq +90^\circ$.

The azimuths (GE) display a spatial variation across the granite and the SET 1 results are subdivided into western and eastern groups in Figure 7. There appears to be a distinction between the azimuths (and rotations with depth) obtained in the extreme west (sites 101 and 102) and the consistent set formed by sites 103, 104, 105, 106 and 107. At site 109 the initial 'swapping' is simply due to +/- azimuth ambiguity but it seems clear that this site (slightly to the south of the main profile) detects a maximum direction that is approximately orthogonal to that at the other sites i.e. it is more 'normally' a *minimum* direction. It is also notable that the azimuth at site 110 rotates below 5 km to a 'minimum direction' similar to that at site 109. The azimuths at the eastern profile sites (110 to 112) display behaviour that is more in character with sites 101 and 102.

It can be seen in Figure 7 that, with the exceptions of sites 109 and 110, the azimuths display a characteristic counterclockwise rotation with depth through the upper crustal section. Although 'local' influences are apparent at the shallowest depths (around 1 km), azimuths appear confined to the NE/ENE sector. In the lower part of the section, azimuths are confined to the N/NE sector. The SET 2 results shown in Figure 7 appear far more stable. This is probably due to their different dimensional characteristics. At site 201 (strong 2-D), a stable depth-independent azimuth is observed. At site 202 (strong 3-D) a straightforward interpretation of a single

horizontal azimuth is probably not possible.

The azimuthal information is generated by the inherent geoelectric anisotropy of the upper crustal section. It is clear from the results presented that the azimuthal information is sensitive to location on the granite. An inherent spatial character both from west to east along the profile and from north to south across the profile is observed. The five central profile sites 103; 104, 105, 106 and 107 appear, however, to form a 'consistent' set of azimuths for the upper crustal section.

4 THE VERTICAL RESISTIVITY PROFILE

The dimensional information considered above revealed that the sounding data on the granite possess a strong 1-D contribution while retaining a relatively constant 2-D influence. The 2-D influence provides anisotropy ratios of between 1.5 and 3.0 through the upper 10 km of the vertical section. The degree of the 1-D influence decreases with increasing depth. In order to provide an assessment of the resistivity/depth profiles for the complete survey, the rotationally invariant, average impedance is used to assess the vertical resistivity profiles.

The 1-D inverse methods used are an attempt to recover the resistivity profile using automatic methods. The sounding data, in this case the average impedance, together with its associated errors are used to provide models that are consistent with the observations at a certain level of misfit. Two inversion schemes have been applied to survey data. The first scheme provides minimum-norm (best-fit) solutions when the section is characterised by a series of layers. The second scheme provides a solution as a smooth resistivity profile at a chosen level of misfit.

The inversion scheme that treats the vertical section as a stack of discrete layers is due to Fischer and Le Quang (1981). As applied here the starting model (the parameters of the crustal section) consists of 5 layers above a uniform half-space of 1000 ohm.m. In each case the minimum-norm solutions are presented which can, if no constraints are applied, provide extreme model behaviour. No constraints other than the initial parameterisation were applied in the present case. Adequate fits to the data were obtained. The measure of misfit used (EPS as defined by Fischer and Le Quang) provided values from 0.030 to 0.050 in the majority of cases.

The results for the SET 1 granite profile sites are shown in Figure 8. The first 'at-surface layer' obtained at some sites is not resolved by the data bandwidth. Within the upper 2 km, a set of excursions to minimum resistivity values (approximately 1000 ohm.m or less) can be noted at a depth of about 1 km. Below a depth of 2 km a pattern of increasing resistivity with depth is broadly observed with the obvious exception of the profile at site 105 (dash line, Fig. 8). Reference to the site location map (Fig. 1) indicates that the relatively low resistivities at this site must occur within a quite localised zone. This spatially unusual result is discussed further during the interpretation.

Below a depth of 2 km individual layer parameters, which involve relatively small resistivity transitions, are not likely to be significant. They are more likely to be the product of differences in data quality and in the applicability of *a priori* assumptions required in 1-D model construction. Despite such 'inversion noise' the resistivity values across the granite are found to increase with depth reaching well-constrained values of between 4,500 and 8,500 ohm.m below a depth of about 7 km.

Although a minimum-norm 1-D inversion should not be attempted for data displaying strong 2-D or 3-D characteristics the results for the SET 2, off-granite sites are shown in Figure 9. The overall oscillatory nature of the solutions can be noted. What is of interest is the transition depth from low resistivities (several hundred ohm.m) to typical granite resistivities (> 1000 ohm.m). The depths at which the transitions occur are arrowed in Figure 9. At site 201 the transition depth occurs at about 1 km while at site 202 the transition occurs at around 1.75 km. If we assume that the low resistivities, in the interval 300 to 400 ohm.m, are associated with the Devonian cover then the transition depth defines the granite contact. Reference to the contour map of the depth to granite compiled by the Camborne School of Mines indicates that the depths (and therefore resistivity of the Devonian cover) can be interpreted in this way.

Since the layered interface-type solutions for the SET 1 profile sites (Fig. 8) do not reveal any spatially-consistent major discontinuities across the upper vertical section, solutions involving only *smooth* behaviour are now considered. The algorithm for generating smooth vertical profiles is the Occam inversion presented by Constable *et al.* (1987). Rather than fitting the sounding data as well as possible (which maximises interface-type behaviour), the smoothest model which fits the data to within an expected tolerance is sought. A 99% confidence level (fitting the whole data to within 3 standard errors) was used here.

The results for the SET 1 profile sites are shown in Figure 10. The result at site 105 is displayed as a dot-dash curve and the results at the eastern-most sites (109-112) are displayed as dash curves. The eastern-most sites, with the exception of site 112, display slightly higher resistivity values than sites to the west. In most respects the solutions obtained are smoothed versions of the previous layered results but are necessarily less well-constrained. Given the results obtained thus far it is extremely tempting to interpret the low resistivity layer (Figure 8) or gradient (Figure 10) observed at some of the sites at a depth of about 1 km. The locations where this behaviour is observed are sites 103, 104, and 105 and 107. The behaviour is most pronounced at sites 103 and 104. Interpretations of the vertical profiles are undertaken at a later stage.

5 BACKGROUND TO THE INTERPRETATION OF RESULTS

Prior to the interpretation of the results a brief background to the interpretation of crustal resistivity variations in crystalline (granitic) rocks is provided. The two main mechanisms requiring consideration are (a) temperature-dependent and (b) pressure-dependent resistivity variations. It should be noted at the outset that the in-situ resistivity will be controlled by the crack and pore parameters of the rock coupled with the fluid content. In order to assess the complete dependence, the effects of temperature and pressure have also to be taken into account.

The temperature dependence of resistivity

In a series of laboratory experiments conducted in the 1960's, Brace and co-workers deduced some of the basic electrical properties of crystalline rocks with low porosities (Brace *et al.* 1965; Brace *et al.* 1968). On the basis of electrical resistivity measurements on rocks saturated with different pore fluids, Brace and his colleagues proposed a model in which the mineral grains act as an insulating matrix and conduction occurs solely through the pore fluid. Thus the effect of temperature is usually incorporated by using the known variation of the pore fluid resistivity with temperature. The empirically determined expression relating fluid resistivity to temperature depends on a set of electrolyte-dependent coefficients (Quist and Marshall 1968). If the pore fluid has a salinity close to seawater then the fluid resistivity (ρ_f) depends on temperature as

$$\rho_f = (3 + T/10)^{-1}$$

(Becker *et al.* 1982) where T is the temperature in degrees Celsius. The relationship is approximately valid up to 300 °C. Using the predicted temperature profile for the Carnmenellis granite (Fig. 2), the expression provides a fluid-resistivity/depth profile as shown in Figure 11. The results indicate a factor of 10 *decrease* in the component of bulk resistivity determined by the fluid phase over the first 10 km of the crustal section.

The influence of the fluid volume may be described either in terms of rock porosity and degree of saturation (e.g. Brace and Orange 1968b) or by the 'weight-percent' of free fluids (e.g. Olhoeft 1981). According to Olhoeft (1981) the electrical properties of granite appear to be dominantly controlled by the amount of *free* water in the granite and by temperature. Near room temperature a monolayer of water will decrease the resistivity by an order of magnitude. A summary of the temperature dependence of 'wet' and 'dry' granite resistivities presented by Olhoeft (1981) is shown in Figure 12. Several weight-percent of water may decrease the resistivity by as much as 9 orders of magnitude. A representative resistivity curve for the Carnmenellis granite is also shown in Figure 12. Depth has been converted to temperature using the results of Figure 2. The highest temperature of 370 °C corresponds to a depth of 10 km. Two main points arise from the comparisons in Figure 12.

The first point is that the observed resistivities of the upper-crustal section are much closer to the 'wet' granite curve than to the 'dry' curve. This 'result' accords with the behaviour of the resistivity laterolog for well RH15 at Rosemanowes quarry which was discussed earlier. Clearly the volume, or bulk, resistivity (as determined by the surface soundings) is determined by the low-resistivity fluid content of fractures and pores within the highly resistive intact matrix. The observed vertical resistivity profiles indicate that this control is maintained down to at least 10 km.

The second point to arise from Figure 12 is that the laboratory temperature dependence gives rise to a decreasing resistivity with increasing temperature, as discussed above. The vertical resistivity profiles require an increasing resistivity with depth (and temperature). Clearly the temperature effect is offset or modified by a more dominant mechanism within the Carnmenellis granite. Mechanisms which would cause an increasing resistivity with depth are discussed below.

The pressure dependence of resistivity

As noted above, the theory of pressure-dependent resistivity in low-porosity rocks, saturated with different pore fluids, was established by Brace and co-workers (Brace *et al.* 1965, 1966, 1968). Specifically, the experiments showed that as the external confining pressure is increased, the resistivity rises sharply and then less so. Their data for the 'typical' response of Westerly granite saturated with 50 ohm.m water are reproduced in Figure 13. The dilatancy of these samples as a function of pressure was also measured. The dilatancy rises sharply with pressure and then asymptotically approaches a straight line. The conclusion was that some of the porosity (called cracks) closes up quickly with pressure while that remaining (called pores) does not. This qualitative picture has since been verified by many other experiments on similar systems. It is important to point out that the definition of 'cracks' and 'pores' (as discussed in the above papers) is in terms of their *response* to pressure or stress. Thus 'cracks' close under applied pressure while 'pores', though free to deform elastically, remain open. Due to the fact that the experiments indicate that a wide range of rock types display this type of behaviour, it is presumed that nearly all rocks must contain high-aspect ratio void spaces that can be closed by applied pressure. Such closure appears to be complete in many granites at around 200 MPa (e.g. Fig. 13 and examples presented by Johnson and Manning 1986). The laboratory observations provide further evidence that *pore* space remains connected in most rocks in spite of deep burial. For example, Brace and Orange (1968b) report that an effective pressure of 1000 MPa was insufficient to eliminate water-filled pore spaces in granitic and other rocks.

For a realistic granite mass, and the Carnmenellis in particular, we should also take into account the likely influence of both the highly jointed nature of the granite and the in situ anisotropic stress distribution. The subject of crustal stress in the UK is receiving growing attention and a recent review is provided by Evans (1987). The review emphasises that the one good quality

stress measurement has been obtained within the Carnmenellis granite (e.g. Fig. 3). Rummel (1986), reviewing European results, quotes the Cornwall results as an extreme case of high deviatoric stress. It appears it is the extremely low minimum horizontal stress that provides the large deviatoric behaviour.

According to conventional laboratory analyses (e.g. Fig. 13) using uniaxial confining pressure, the transfer from crack-dominated behaviour to pore-dominated behaviour will occur at modest lithostatic pressures of about 200 MPa. However at this point it is possible to suggest that the *in-situ* rock-mass behaviour can be described by the dilatant growth and alignment of microcracks which are kept open by pore-fluids at high pressures as described by Brace and his colleagues (Brace and Byerlee 1967; Brace and Orange 1968a; Walsh 1965) and as more recently advocated by Crampin (1985) and by Crampin and Atkinson (1985). The extended theory of Extensive Dilatancy Anisotropy (EDA) has been examined using shear-wave splitting for the Carnmenellis granite by Roberts and Crampin (1986). Their results suggest the mean direction of maximum horizontal stress is 30° west and is therefore parallel to one of the principal joint sets observed at the surface (JOINT SET 1, Fig. 3).

Relatively little work has been developed to relate the implications of the EDA hypothesis to geoelectric behaviour. This is, in part, due to the large influence of *structural* (or macroscopic) anisotropy on geoelectric sounding data. In the absence of such anisotropy a qualitative guide to the likely effects is now suggested. The pressure dependence of granite resistivity, shown in Figure 13, displays a sensitive, non-linear relationship in the region of laboratory crack-dominated behaviour (e.g. 0 to 200 MPa). This simple uniaxial dependence would then form a model for deviatoric differences due to an anisotropic stress field. We therefore superimpose an existing stress field with magnitude axes s_H (maximum horizontal, acting at θ_H), s_h (minimum horizontal, acting at θ_h) and s_v (vertical). Using Figure 13 we can visualise a situation ($s_H \neq s_h \neq s_v$) which will generate substantial resistivity variations depending on the relative magnitudes of the inequalities. Clearly for a horizontally dominant stress field, *maximum* resistivities will be generated (by s_H) at an azimuth θ_H . For this situation, the degree of resistivity anisotropy will be related to the ratio s_H/s_h .

6 INTERPRETATION OF LATERAL GEOELECTRIC ANISOTROPY

This section describes the extent to which the granite can be considered laterally homogeneous in terms of its rock/fluid electrical properties across the survey area. The results relevant to this interpretation are the dimensional and rotational characteristics that have been presented. It can be noted that for sites on the granite the anisotropy ratios are remarkably consistent and form a set of values in the range 1.5 to 3 (see Fig. 6). The azimuths of maximum resistivity (GE) shown in Figure 7 display a consistent rotation pattern from NE/ENE at shallow depths to N/NE at a depth of 10 km.

The rotation with depth across the upper vertical section is likely to be due to the transition from near-surface to more regional influences. The near-surface hydrogeological model of the granite (Burgess *et al.* 1982) implies a saline water circulation system down to a depth of 1.1 km and suggests that the joint/fracture system extends to 2 km or more. Gregory and Durrance (1987) extend the hydrogeological model further (using the distribution of radioelement concentrations) and propose and map an active hydrothermal circulation system across the Carnmenellis structure.

According to Gregory and Durrance (1987), where a system of hydrothermal convective circulation operates in a well-fractured granite such as the Carnmenellis, the spatial distribution of these cells is likely to be closely tied to the distribution of major water-conducting features. In this context, fractures include all classes of physical break within the granite, such as joints and faults, whether mineralised or barren. The pattern of jointing within the Carnmenellis is generally described by two sets of master joints trending NE-SW and NW-SE (see Fig. 3). The borehole information considered by Heath (1985) indicated that in the upper 200m the water-conducting fractures were dominantly orientated NW-SE, but below this zone the preferred orientations change with depth. Larger scale faults cutting the Carnmenellis generally run parallel to the master joints with the NW-SE trend dominant. The NW-SE faults are part of a major series of strike-slip displacements which occur throughout southwest England (Dearman 1963).

Gregory and Durrance (1987) suggest that, on uplift, fractures which trend approximately NW-SE will open, while NE-SW fractures will remain closed. Since the principal stress directions differ from the azimuths of the two joint sets, it may be possible to use this fact as a constraint in relation to the observations of resistivity anisotropy. Using the previous examples of control of resistivity anisotropy due to pressure dependence two distinct effects could be anticipated. If simple and spatially persistent jointing controls the resistivity anisotropy the azimuths of maximum resistivity could be expected to be perpendicular to the direction of the major fluid-filled joints. Thus if a NW-SE joint set is the major fluid-filled feature within the granite the azimuth of maximum resistivity would be NE-SW. If however the resistivity anisotropy is controlled by microcracks we would anticipate maximum and minimum resistivity azimuths to be controlled by the principal stress directions, as discussed previously.

To provide diagnostic information on the possible influences, the azimuths of maximum resistivity are shown in relation to the joint/stress directions in Figure 14 for three frequencies (penetration depths). At the first frequency (89.5 Hz), penetration depths range from 832 m (at site 106) to 1686 m (at site 110). For the second frequency (8.95 Hz) penetration depths are predominantly in the range 3 to 6 km and for the third frequency (0.089 Hz) penetration depths are greater than 25 km.

The counterclockwise rotation with decreasing frequency can be observed in Figure 14. The directions of maximum resistivity shown in Figure 14a show reasonably consistent orientations

that are predominantly parallel to JOINT SET 2 (60 to 90 degrees). This result suggests that within the upper 1.5 km, resistivity may be controlled by joint (as opposed to stress) related effects. In this case the predominant fluid-filled joint system would have a strike approximately parallel to JOINT SET 1. The results for a frequency of 8.95 Hz refer to a deeper penetration radius of between 3 and 6 km. The counterclockwise rotation is part of a continuous rotation with increasing penetration radius. The main conclusion from Figure 14b is that there is no evidence of any alignment with the principal stress directions (see Fig. 14c). Increasing the penetration radius beyond 25 km (a frequency of 0.089 Hz) provides a reasonably consistent set of azimuths which again do not display any alignment with the principal stress directions. There *appears* rather to be a correlation between the azimuths of maximum resistivity and the strike direction of JOINT SET 1. It must be noted however that this correlation may be 'coincidental' since the anisotropy at this radius refers to a substantial volume of the granite and root batholith. The azimuths obtained are also approximately normal to a set of regional thrust faults to the south and east of the outcrop (the Carrick, Lizard and Dodman thrust faults). It is suggested that an unambiguous 'regional' interpretation is not possible using the results of a spatially limited experiment.

The vertical resistivity profiles presented in Figures 8 and 10 also provide controls on the lateral homogeneity of the granite. The resolution of the data in the upper 1 km is difficult to determine. The at-surface resistivity of each solution depends on high-frequency asymptotic behaviour 'extrapolated' by the minimisation. It should therefore be appreciated that the 'definition' of this layer/gradient depends primarily on the extrapolated value of the at-surface resistivity. At present we have no way of confirming the at-surface values obtained. At two locations (sites 105 and 106) however, consistently low at-surface resistivities (of order 500 ohm.m) are observed. Reference to the site locations in relation to the main alluvial fans crossing the area shows that these two sites are indeed the only two sites situated centrally within major fans. Reference to the regional geological maps confirms that the fans in question provide major arterial connections to the coast. Of the two sites in question, site 105 is situated on Porkellis moor which, in volumetric terms, appears to represent the main alluvial 'basin' on the granite. The trend of the fan coastwards (NE-SW) also represents one of the main NE-SW trending lineaments on the Carnmenellis structure. It is suggested that the relatively low resistivity values obtained at site 105 are due to the spatially localised influence of the alluvial fan and/or associated lineament. With the possible exception of this site, the uniformity of dimensional information, coupled with the common behaviour of resistivity values below a depth of 2 km, suggests that the surface lineations, traversed by the main survey profile, do not represent 'super-deep' continuous fractures.

7 INTERPRETATION OF THE VERTICAL CRUSTAL SECTION

The dimensional information considered previously revealed that the sounding data on the granite possess a strong 1-D influence. This information alone testifies to the overall 'homogeneity' of

the granite mass defining the Carnmenellis outcrop. The data for the two off-granite soundings (sites 201 and 202) display significant 2-D and 3-D influences and so a recovery of their complete vertical profiles is not simple. The results of Figure 9 indicate however that the data detect the cover/granite contact.

With the exception of site 105, the overall set of 1-D solutions (Figures 8 and 10) provide a very consistent profile of the deep resistivity structure of the Carnmenellis granite. Typical resistivities at a depth of 1 to 2 km are in the range 1000 to 2000 ohm.m. The resistivity increases slowly with depth reaching values approaching 10,000 ohm.m at a depth of 10 km. Although such a small but steady increase is difficult to resolve, maximum resistivity values are apparent in the depth range 4 to 6 km. The observed resistivity values correspond to a 'wet' granite saturated with several weight-percent of water; a mechanism that is maintained down to at least 10 km.

Of direct interest to the interpretation of the upper crustal section are the wide-angle seismic reflection results of Brooks *et al.* (1984) and the two reflectors (R1,R2) discussed previously. The shallowest reflector (R1) was observed at a depth of about 7 to 8 km and appears to be confined to the granite. The model reflector R1 defines the upper surface of a low-velocity zone which extends to the second reflector (R2) in the depth interval 12 to 15 km. The interpretations considered by Brooks *et al.* (1984) were confined to the nature of the horizons rather than the nature of the low velocity zone which defines the horizons. The most direct 'interface' comparison is with the minimum-norm, layered resistivity profiles of Figure 8. For these solutions individual layer parameters which involve small resistivity contrasts are not likely to be significant. The solutions obtained do not reveal any spatially consistent major discontinuities across the vertical section. Instead it can be noted that the depth interval of the low-velocity zone appears to be associated with an interval of approximately constant and maximum resistivity. Thus no detectable variations in rock/fluid properties can be identified at depths that might be associated with the R1 reflector. In geoelectric terms then, R1 does not appear to represent a fractured zone with an associated enhancement of conducting fluids.

We now turn to the task of assessing the mechanism which controls the depth dependence of resistivity behaviour. Thermal control of resistivity does not appear to be the dominant mechanism. It has been suggested that the pressure dependence of resistivity must account for the observed increase in resistivity with depth. The vertical resistivity profiles (Figures 8 and 10) demonstrate that the physical mechanism producing the depth dependence appears spatially consistent from west to east across the granite. Refinements to the interpretation are difficult since most laboratory analyses deal only with uniaxial pressure i.e. lithostatic load.

The most relevant laboratory resistivity experiments to which such observations can be related are those of Trimmer *et al.* (1980) who studied the effect of pressure and stress on water transport in intact and fractured granite. Some conductance (i.e. normalised conductivity) measurements were made during the course of the experiments. The measurements were limited to pressure/stress magnitudes of less than 40 MPa (equivalent to depths of less than 2 km), but the

results may have broader application. Trimmer *et al.* (1980) note that throughgoing fractures in Westerly granite dominate water transport, increasing the permeability by 6-9 orders of magnitude when compared with intact rocks. Observed changes in conductance, where available, mirror changes in permeability. Overall the data on both intact and *fractured* rock are consistent with previous experiments of crack closure and dilatancy both with and without differential stress. The previous experiments referred to are those of Brace *et al.* (1968) and Brace and Orange (1968b). The Brace model thus appears to hold for fractured and stressed rock.

The deep observations of jointing and stress characteristics within the Carnmenellis granite are obviously limited to borehole information. It is known from the Rosemanowes borehole logs that the jointing exists to at least 2.5 km and we can infer from the microseismicity that it persists to a depth of 4 km. The variation of the magnitude of the stress components has been estimated to a depth of around 2.5 km (Green *et al.* 1987). Clearly the borehole observations must be extrapolated to provide deeper information. If all other possible effects are ignored then the linearly extrapolated stress magnitudes at a depth of 6 km are 180 MPa for the maximum horizontal stress, 150 MPa for the overburden stress and 80 MPa for the minimum horizontal stress.

The fundamental resistivity/pressure dependence of low-porosity granitic rocks has been summarised in Figure 13. According to the original work of Brace *et al.* (1965) and all other subsequent experiments, the point of inflection between the initial non-linear response and the subsequent high-pressure linear response corresponds to the transfer from crack-dominated behaviour to pore-dominated behaviour. According to Figure 13, the transition should be complete and all forms of cracks should be closed at pressures of approximately 200 MPa. The extrapolated measurements for the maximum horizontal stress field within the Carnmenellis granite clearly approach this value at a depth of 6 km which, in addition, also corresponds to the depth of maximum resistivity observed across the granite. The resistivity profiles obtained appear therefore to 'reflect' (i.e. are consistent with) the completion of crack closure at a depth of about 6 km and a transfer to a pore-dominated resistivity mechanism below this depth. *Thus in very simplistic terms*, if a joint can be defined as a feature that is capable of 'closing' (and closed here means an inability to support ionic conduction of interstitial fluids) then the above observations suggest the absence of such joints below 6 km.

8 CONCLUSIONS

Overall the Carnmenellis granite, as defined by its broad resistivity characteristics, appears predominantly homogeneous. A consistent set of resistivity values are found for the whole granite structure below a depth of 2 km. The majority of resistivity values are in the range 1,000 to 10,000 ohm.m. When laboratory analyses of thermal and pressure dependence are taken into account the granite is found to correspond to a 'wet' granite saturated with several

weight-percent of free solutions down to at least 10 km.

The consistency of the resistivity values below 2 km across a major portion of the granite indicates that lateral geoelectric effects are confined to the near-surface (i.e. < 2 km). The results relating to the lateral anisotropic behaviour confirm this general conclusion. With the exception of one location surface lineations, across the survey profile, do not appear to represent 'super-deep' vertical or sub-vertical zones with rock/fluid properties that would distinguish them from 'background' behaviour. The anomalous conductive zone appears to be correlated with a lineament and a main arterial alluvial fan. The E-W survey profile intersects this NE-SW trending zone some 0.5 km directly south of the village of Porkellis. The location also coincides with an area of past ore-mining activity.

The information on geoelectric anisotropy has been compared with the principal joint and stress directions of the granite in order to identify the mechanism controlling the resistivity anisotropy. The main conclusion is that the directions of resistivity anisotropy do not display any persistent alignment with the principal horizontal stress directions. Such a conclusion assumes that the present indicators of stress directions are representative of the *in situ* stress at depths in excess of 2 km. On this basis the mechanism of aligned microcracks does not appear to control the geoelectric anisotropy. The results indicate that within the upper 1.5 km (at least), resistivity is controlled by one of the two principal joint systems of the granite. The results identify the fracture system parallel to the NW-SE master joints as being preferentially 'open' and containing enhanced concentrations of fluids.

The vertical resistivity profiles have been compared with boundary reflector (R1) of the low-velocity zone modelled by Brooks *et al* (1984). The resistivity profiles do not reveal any spatially consistent major discontinuities at the appropriate depth. The depth interval of the low-velocity zone appears merely to be associated with an interval of approximately constant and maximum resistivity. Thus the reflector R1 does not appear to represent the upper surface of a fracture (thrust) zone with an associated enhancement of conducting material.

Below a depth of 2 km resistivity values increase slowly with depth attaining maximum values by about 6 km. The anticipated decrease of resistivity values with increasing depth and temperature is not observed and a more dominant pressure/stress dependence must control the spatially consistent depth dependence observed. Laboratory measurements on a wide range of granitic rocks indicate that transfer from crack-dominated behaviour to pore-dominated behaviour will be complete at applied pressures of about 200 MPa. The extrapolated overburden and stress magnitudes, from borehole measurements, suggest that this will be achieved within the Carnmenellis granite by about 6 km. The resistivity profiles are therefore consistent with the completion of joint and crack closure by a depth of around 6 km and a transfer to a pore-dominated resistivity mechanism below this depth.

ACKNOWLEDGEMENTS

It is a pleasure to acknowledge the friendly assistance of the many farmers of the Carnmenellis area who granted land-access during the fieldwork. Scott Finnie proved a very capable field-assistant and his fortitude is gratefully acknowledged. The staff of the Camborne School of Mines, Geothermal Energy Project at Rosemanowes Quarry provided facilities and advice for which I am grateful. Their faith in the applicability of the technique is much appreciated. The work described in this report was funded under a contract from the Camborne School of Mines, Geothermal Energy Project (Department of Energy). This report is published with the approval of the Director, British Geological Survey (NERC).

REFERENCES

- Anon., 1987. Hot Dry Rock potential of the United Kingdom, *Invest. Geotherm. Potent. U.K.*, British Geological Survey.
- Batchelor, A.S., 1984. Hot dry rock geothermal exploitation in the United Kingdom, *Mod. Geol.*, 9, 1-41.
- Beamish, D., 1986. Geoelectric structural dimensions : methods of estimation, old and new, *Geophysics*, 51, 1298-1309.
- Beamish, D. and Riddick, J.C., 1989. An audiomagnetotelluric survey of the Carnmenellis granite, *British Geological Survey, Scientific Report*, SM/89/15.
- Becker, K., Von Herzen, R.P., Francis, T.J.G., Anderson, R.N., Honnorez, J., Adamson, A.C., Alt, J.C., Emmermann, R., Kempton, P.D., Kinoshita, H., Laverne, C., Mottl, M.J. and Newmark, R.L., 1982. *In situ* electrical resistivity and bulk porosity of the oceanic crust Costa Rica Rift, *Nature*, 300, 594-598.
- Brace, W.F., Orange, A.S. and Madden, T.R., 1965. The effect of pressure on the electrical resistivity of water-saturated crystalline rocks, *J. Geophys. Res.*, 70, 5669-5678.
- Brace, W.F., Paulding, B.W. and Scholz, C., 1966. Dilatancy in the fracture of crystalline rocks, *J. Geophys. Res.*, 71, 3939-3953.
- Brace, W.F. and Byerlee, J.D., 1967. Recent experimental studies of brittle fracture in rocks, in *Failure and Breakage of Rock*, American Institute of Mining, New York, 58-81.
- Brace, W.F. and Orange, A.S., 1968a. Electrical resistivity changes in saturated rocks during fracture and frictional sliding, *J. Geophys. Res.*, 73, 1433-1445.
- Brace, W.F. and Orange, A.S., 1968b. Further studies of the effect of pressure on electrical resistivity of rocks, *J. Geophys. Res.* 73, 5407-5420.
- Brace, W.F., Walsh, J.B. and Frangos, W.T., 1968. Permeability of granite under high pressure, *J. Geophys. Res.*, 73, 2225-2236.
- Brooks, M., Doody, J.J. and Al-Rawi, F.R.J., 1984. Major crustal reflectors beneath SW England, *J. Geol. Soc. Lond.*, 141, 97-103.
- Burgess, W.G., Edmunds, W.M., Andrews, J.N., Kay, R.L.F. and Lee, D.J., 1982. The origin and circulation of groundwater in the Carnmenellis granite : the hydrogeochemical evidence, *Invest. Geotherm. Potent. U.K.*, British Geological Survey.
- Constable, S.C., Parker, R.L. and Constable, C.G., 1987. Occam's inversion : A practical algorithm for generating smooth models from electromagnetic sounding data, *Geophysics*, 52, 289-300.
- Crampin, S., 1985. Evidence for aligned cracks in the Earth's crust, *First Break*, 3, 12-15.
- Crampin, S. and Atkinson, B.K., 1985. Microcracks in the Earth's crust, *First Break*, 3, 16-20.
- Dearman, W.R., 1963. Wrench faulting in Cornwall and south Devon, *Proc. Geol. Assoc.*, 74, 265-287.
- Edmunds, W.M., Andrews, J.N., Bromley, A.V., Kay, R.L.F., Milodowski, A., Savage, D. and Thomas, L.J., 1988. Granite-water interactions in relation to Hot Dry Rock geothermal development, *Invest. Geotherm. Potent. U.K.*, British Geological Survey.
- Eggers, D., 1982. An eigenstate formulation of the magnetotelluric impedance tensor, *Geophysics*, 47, 1204-1214.

- Evans, C.J., 1987. Crustal stress in the United Kingdom, *Invest. Geotherm. Potent. U.K.*, British Geological Survey.
- Fischer, G. and Le Quang, B.V., 1981. Topography and minimisation of the standard deviation in one-dimensional magnetotelluric modelling, *Geophys. J. R. astr. Soc.*, **67**, 257-278.
- Gamble, T.D., Goubau, W.M. and Clarke, J., 1979. Error analysis for remote reference magnetotellurics, *Geophysics*, **44**, 959-968.
- Green, A.S.P., Baria, R. and Jones, R., 1987. Fault-plane analysis of microseismicity induced by fluid injections into granite, in *Engineering Geology of Underground Movements*, eds., Bell, F.G. and Cripps J.C., Proc. 23rd Ann. Conf. Engineering Group Geol. Soc., Nottingham University.
- Gregory, R.G. and Durrance, E.M., 1987. Helium, Radon, and hydrothermal circulation associated with the Carnmenellis radiothermal granite of southwest England, *J. Geophys. Res.*, **92**, 12567-12586.
- Heath, M.J., 1985. Geological control of fracture permeability in the Carnmenellis granite, Cornwall: implications for radionuclide migration, *Mineral. Mag.*, **49**, 233-244.
- Lee, M.K., 1986. Hot Dry Rock, in *Geothermal Energy-the Potential of the United Kingdom*, eds., Downing, R.A. and Gray, D.A., HMSO, London, 21-41.
- Johnson, D.L. and Manning, H.J., 1986. Theory of pressure dependent resistivity in crystalline rocks, *J. Geophys. Res.*, **91**, 11611-11617.
- Olhoeft, G.R., 1981. Electrical properties of granite with implications for the lower crust, *J. Geophys. Res.*, **86**, 931-936.
- Quist, A.S. and Marshall, W.L., 1968. Electrical conductances of aqueous sodium chloride solutions from 0 to 800° and at pressures to 4000 bars, *J. Phys. Chem.*, **73**, 978-985.
- Roberts, G. and Crampin, S., 1986. Shear wave polarisations in a Hot Dry Rock Geothermal Reservoir : Anisotropic effects of fractures, *Int. J. Rock Mech. Min. Sci & Geomech. Abstr.*, **23**, 291-302.
- Rummel, F., 1986. Stresses and tectonics of the upper continental crust : a review, in *Proceedings of the International Symposium on Rock Stress and Rock Stress Measurements*, ed., Stephenson, O., Stockholm, 177-186.
- Sams, M.S. and Thomas-Betts, A., 1988. 3-D numerical modelling of the conductive heat flow of SW England, *Geophys. J.*, **92**, 323-334.
- Schmucker, U., 1987. Substitute conductors for electromagnetic response estimates, *Pageoph.*, **125**, 341-367.
- Telford, W.M., Geldart, L.P., Sheriff, R.E. and Keys, D.A., 1976. *Applied Geophysics*, Cambridge University Press.
- Travassos, J.M. and Beamish, D., 1988. Magnetotelluric data processing - a case study, *Geophys. J.*, **93**, 377-391.
- Trimmer, D., Bonner, B., Heard, H.C. and Duba, A., 1980. Effect of pressure and stress on water transport in intact and fractured gabbro and granite, *J. Geophys. Res.*, **85**, 7059-7071.
- Tzanis, A., 1987. Investigations on the properties and estimation of earth response operators from EM sounding data, *PhD thesis*, University of Edinburgh.
- Walsh, J.B., 1965. The effect of cracks on the uniaxial elastic compression of rocks, *J. Geophys. Res.*, **70**, 399-411.
- Walsh, J.B. and Brace, W.F., 1984. The effect of pressure on porosity and the transport

properties of rock, *J. Geophys. Res.*, 89, 9425-9431.

Weidelt, P., 1972. The inverse problem of geomagnetic induction, *J. Geophys.*, 41, 85-109.

Wheildon, J. and Rollin, K.E., 1986. Heat flow, in *Geothermal Energy-the Potential of the United Kingdom*, eds., Downing, R.A. and Gray, D.A., HMSO, London, 8-20.

Willis-Richards, J., 1986. Three-dimensional modelling from gravity of the Carnmenellis granite pluton, West Cornwall, *Geophys. J. R. astr. Soc.*, 74, 251 (Abstract).

Word, D.R., Smith, H.W. and Bostick, F.X. Jr., 1970. An investigation of the magnetotelluric tensor impedance method, *Tech. Rep. 82*, Electr. Geophys. Res. Lab., Univ. of Texas at Austin.

Table 1. Summary of survey site locations in National Grid coordinates (Reference SW) in units of 0.1 km and site elevations in metres.

SITE	EASTING	NORTHING	ELEVATION
101	663	322	150
102	680	320	140
103	685	325	125
104	689	313	173
105	694	327	125
106	708	320	140
107	716	320	185
108	716	323	182
109	724	303	145
110	742	323	175
111	753	325	145
112	764	322	100
201	625	306	97
202	716	276	70

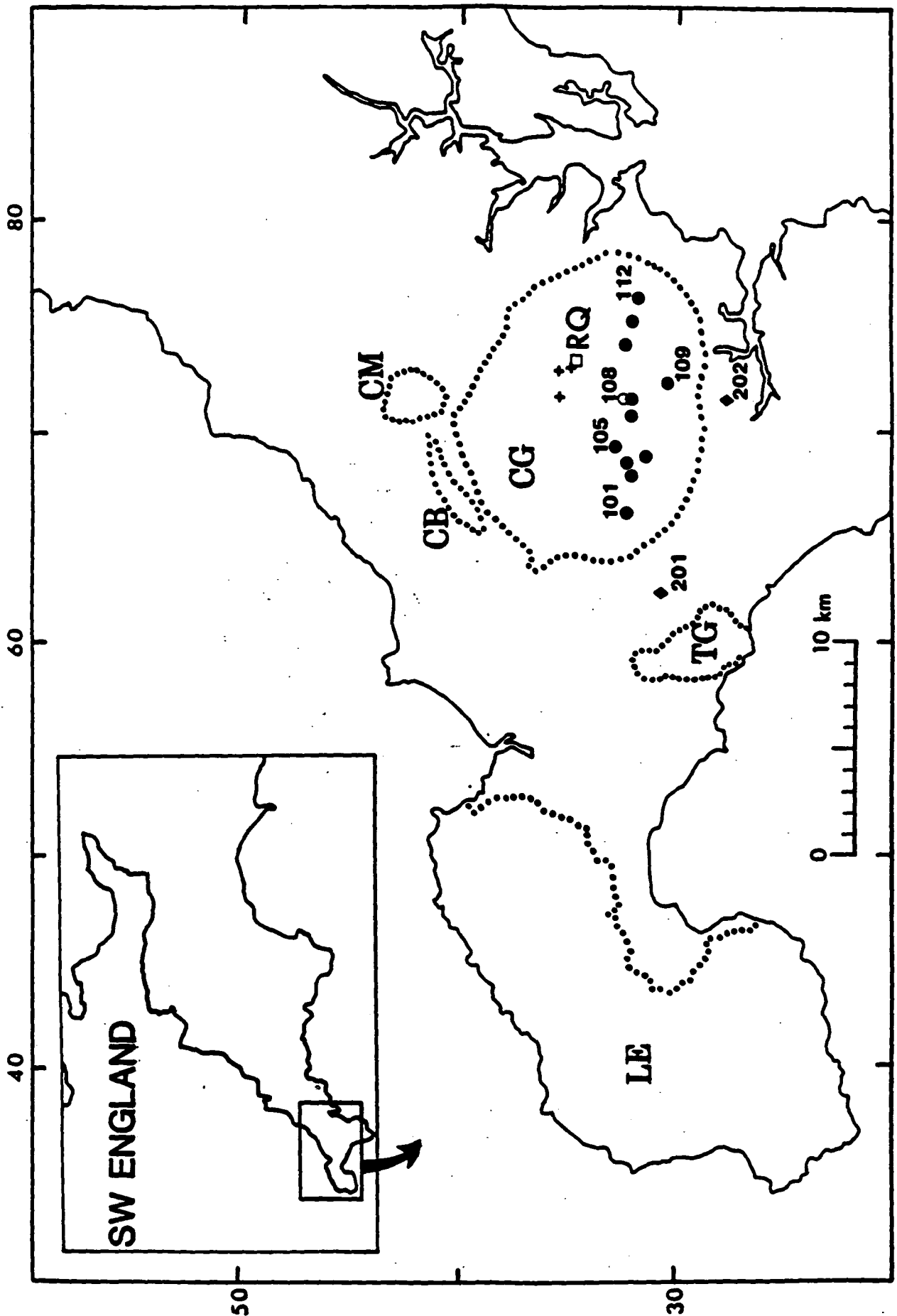


Figure 1. Survey location map. Granite outcrop boundaries are shown dotted. CG=Carnmenellis granite, LE=Land's End granite, TG=Tregonning-Godolphin outcrop, CB=Carn Brea outcrop, CM=Carn Marth outcrop. SET 1 survey sites (101 to 112, site numbers increasing easterly) are shown as solid circles except site 108 (open circle) not used here. SET 2 survey sites (201 and 202), off the main CG outcrop, are shown as diamonds. The location of the HDR test site at Rosemanowes quarry is RQ (open square).

< PREDICTED TEMPERATURE PROFILE >

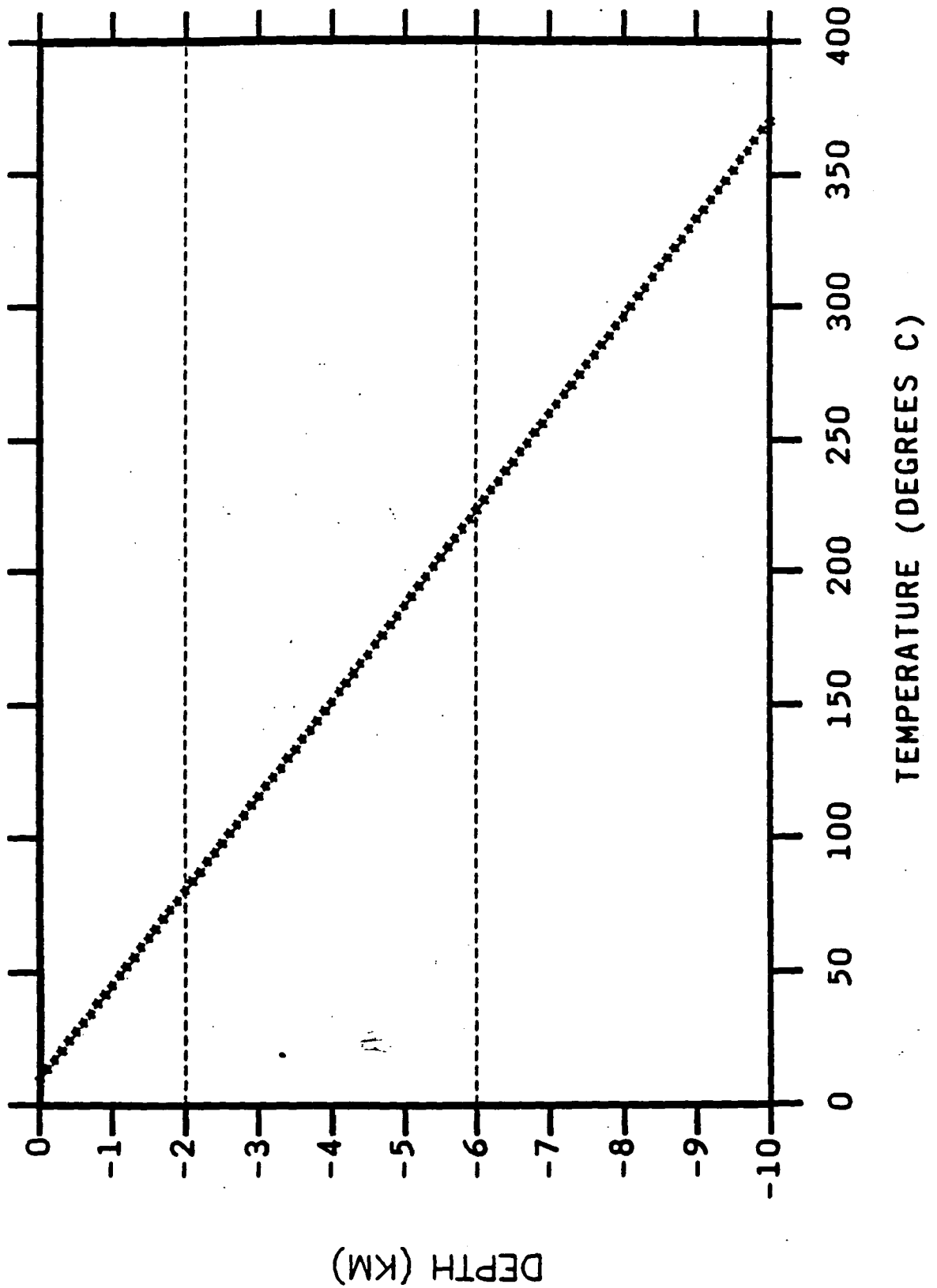


Figure 2. Predicted temperature-depth profile for the Carnmenellis granite calculated from a 1-D heat transfer model. The parameters used in the model are those of Wheildon and Rollin (1986) and Lee (1986).

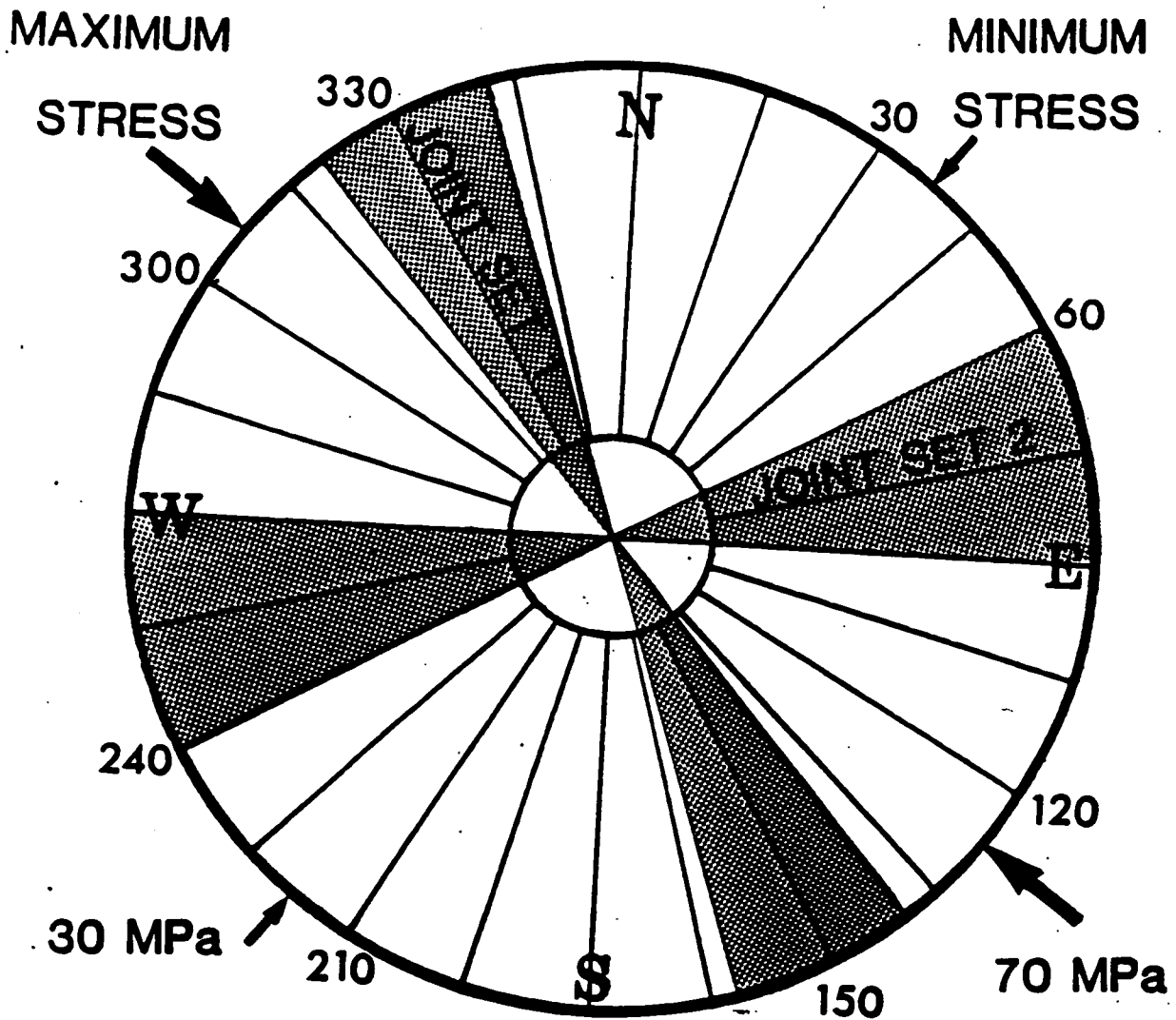


Figure 3. Summary of the orientations of surface joint sets (JOINT SETS 1 and 2) and the horizontal stress field directions and magnitudes at a depth of 2 km. After Batchelor (1984) and Green *et al.* (1987).

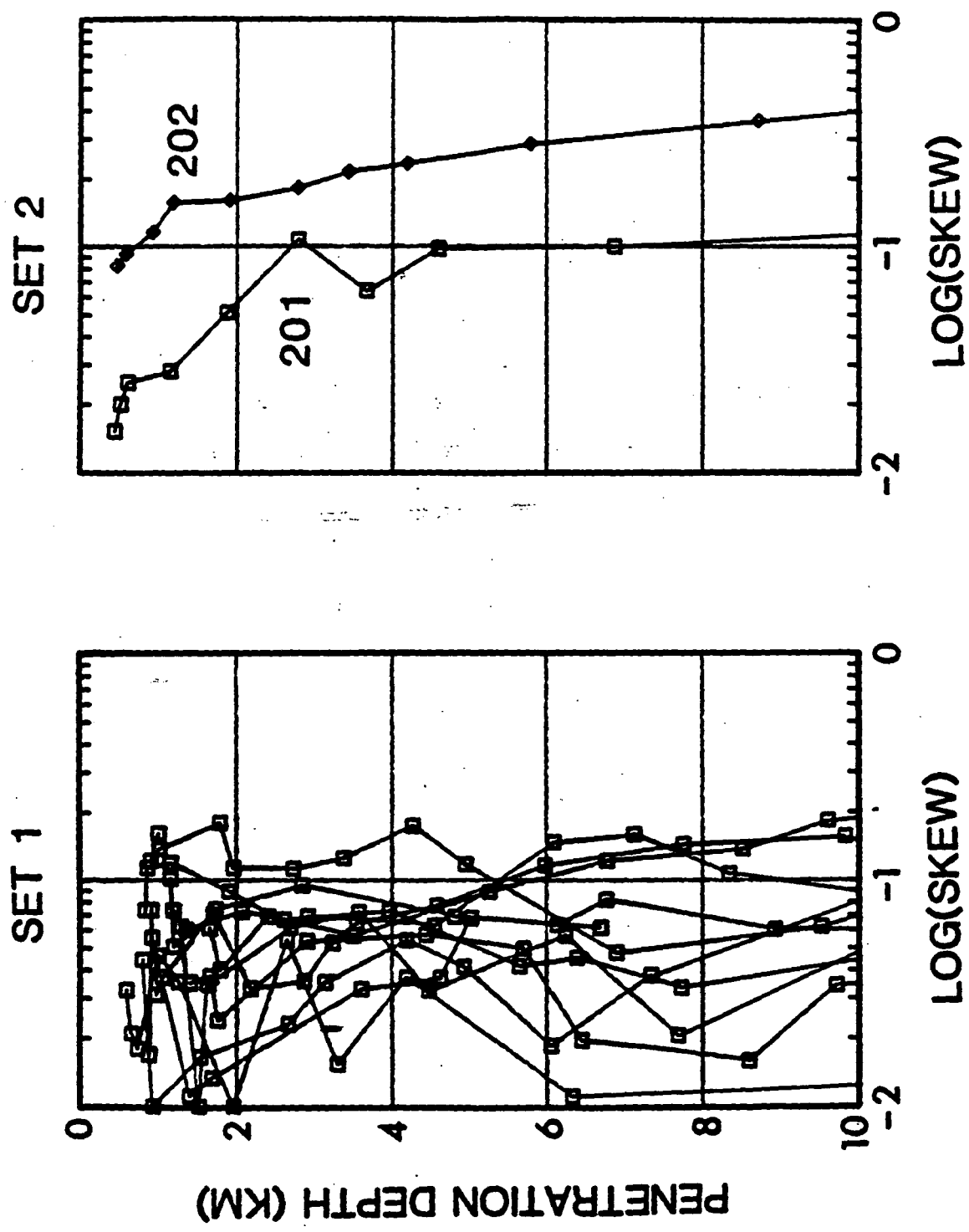


Figure 4. Skew values (logarithmic scale) for the SET 1 and SET 2 survey locations. Plotted as a function of penetration depth (see text).

(a) SET 1 DIMENSIONAL WEIGHTS

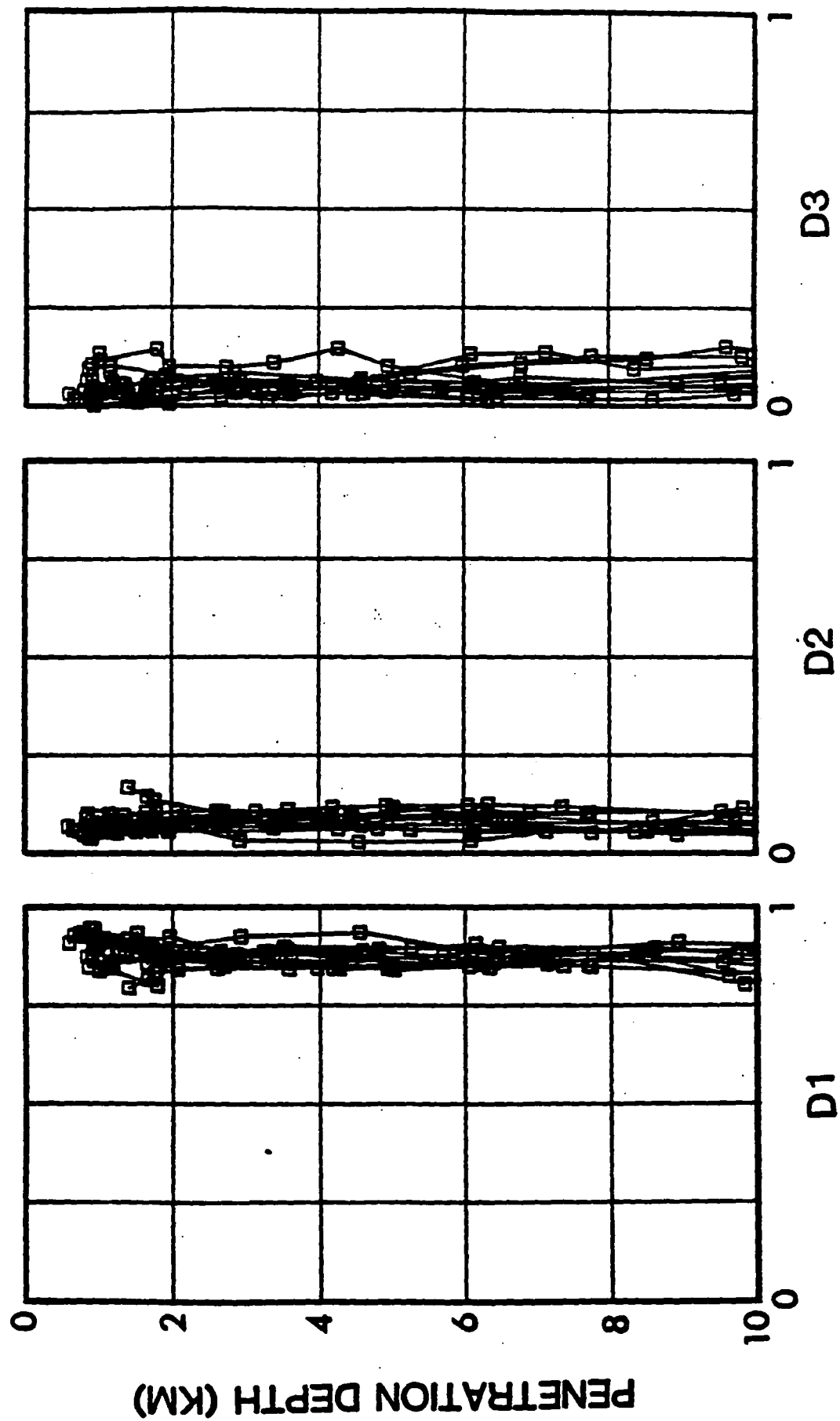
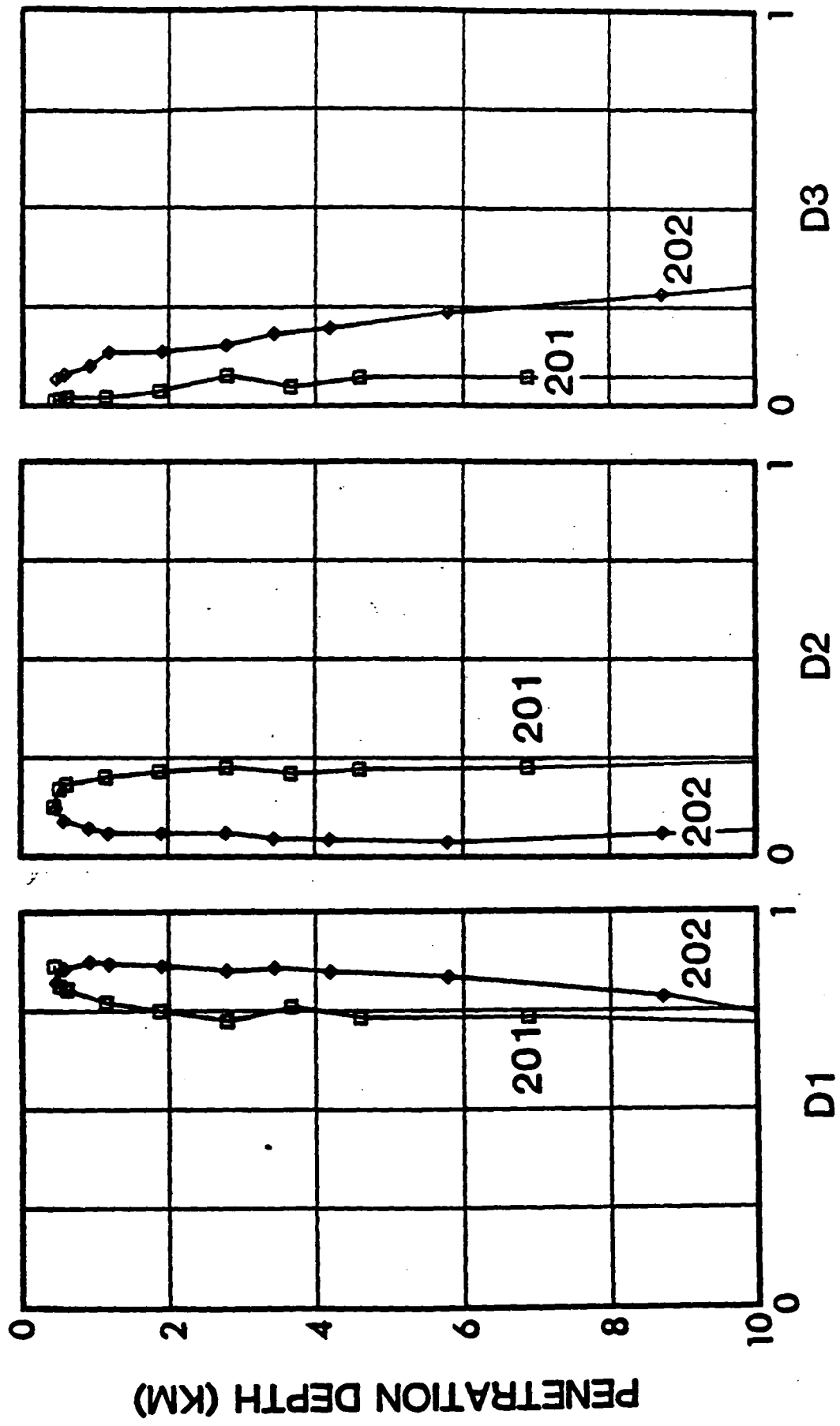


Figure 5. Dimensional weights D1 (1-D), D2 (2-D) and D3 (3-D) for the SET 1 (Fig. 5a) and SET 2 (Fig. 5b) survey locations. Plotted as a function of penetration depth (see text).

(b) SET 2 DIMENSIONAL WEIGHTS



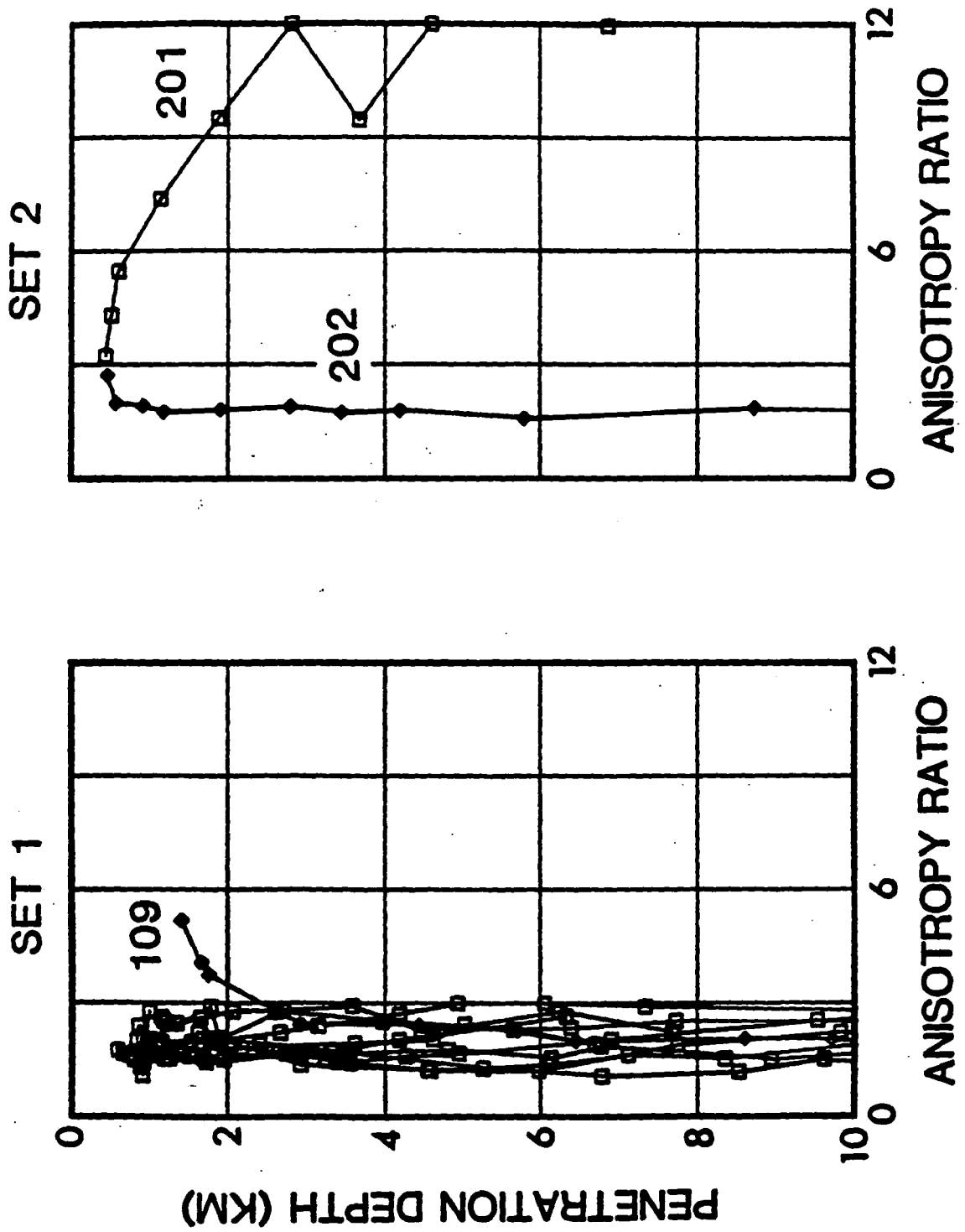


Figure 6. Resistivity anisotropy ratios for the SET 1 and SET 2 survey locations. Plotted as a function of penetration depth (see text).

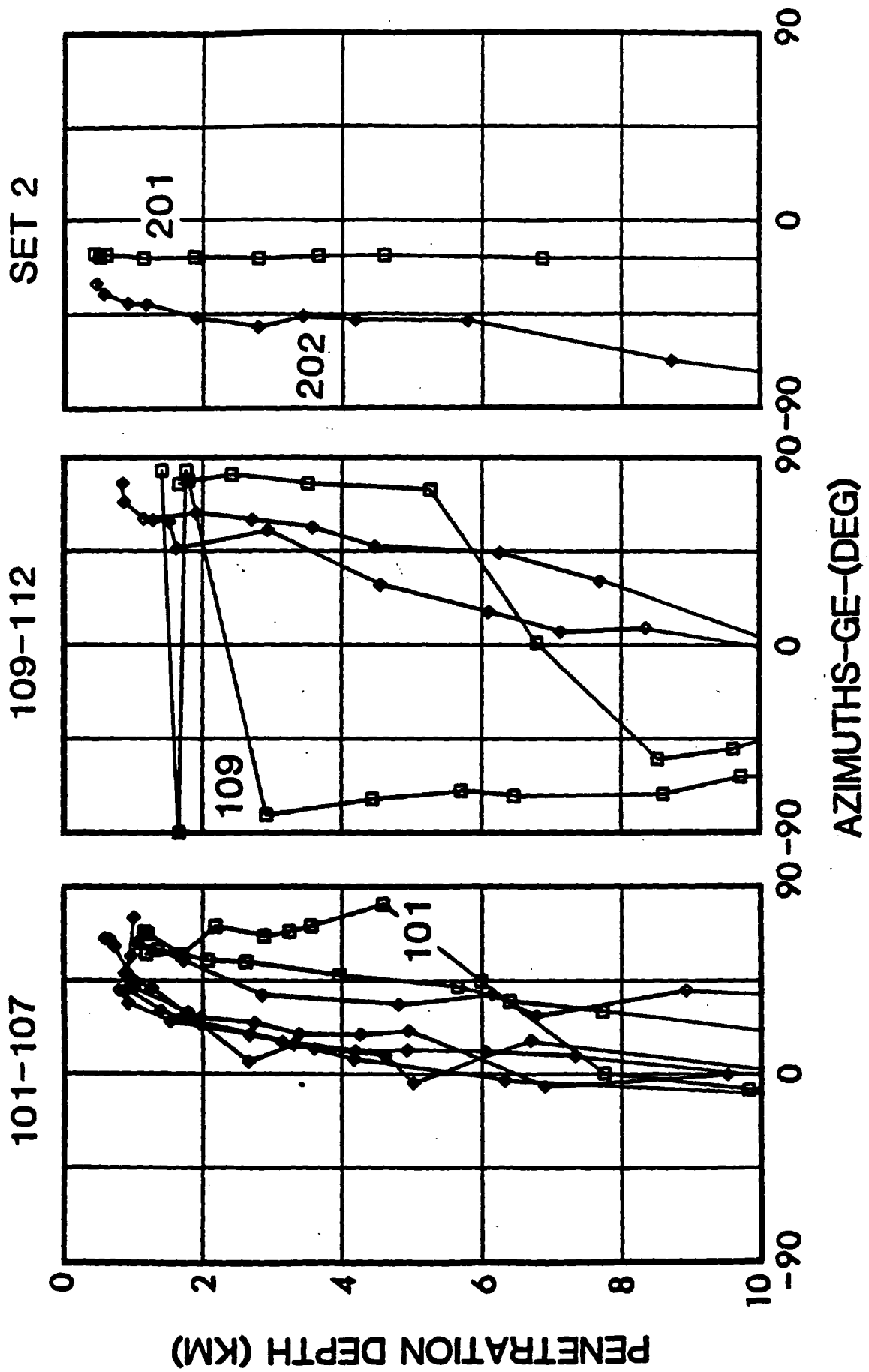


Figure 7. Azimuths of maximum resistivity for the SET 1 and SET 2 survey locations. SET 1 results subdivided into a western group (sites 101-107) and an eastern group (sites 109-112). Plotted as a function of penetration depth (see text).

LAYERED MODELS ACROSS THE GRANITE

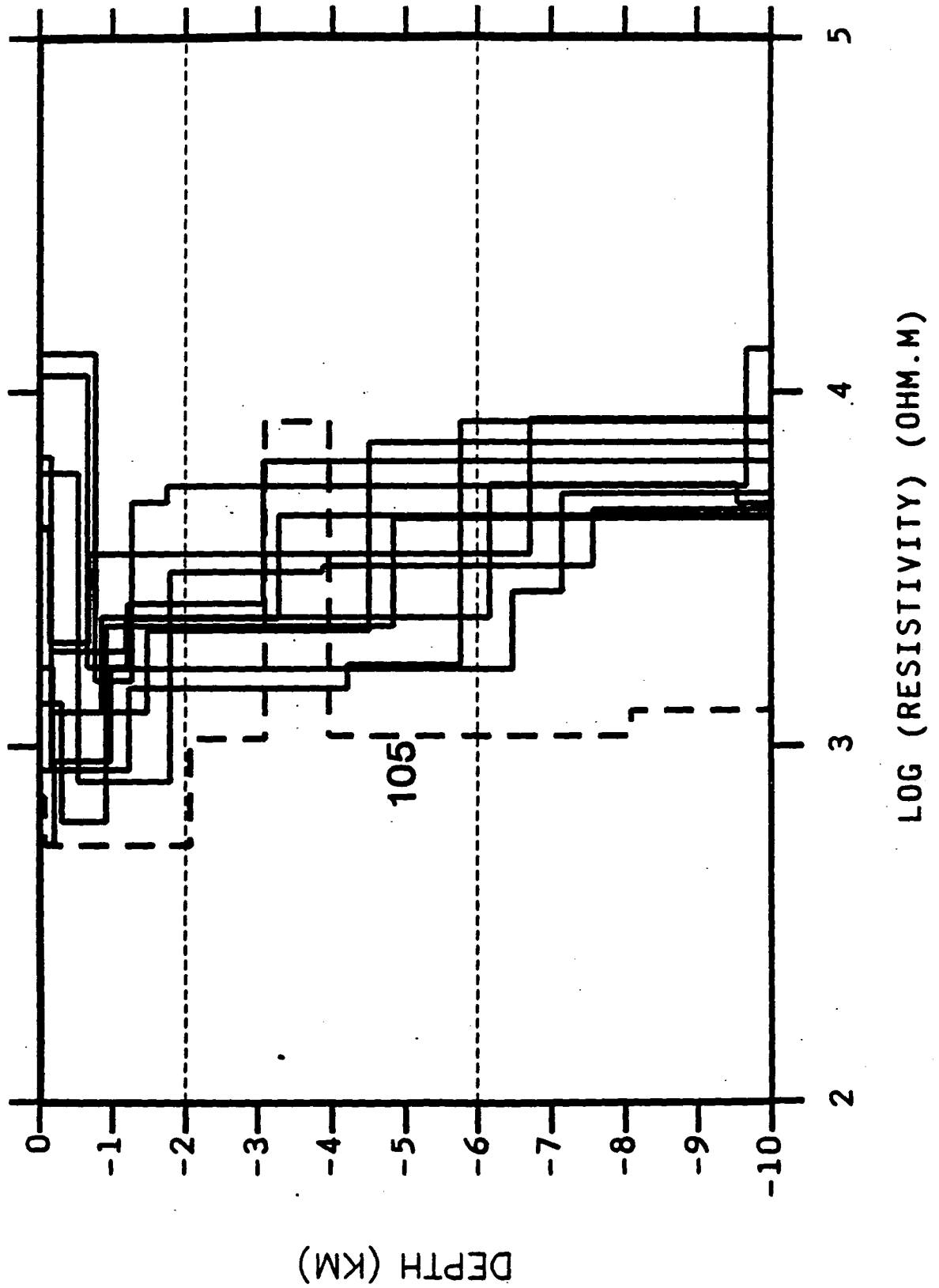


Figure 8. 1-D inversion results (layered models) for the SET 1 profile sites. The lower resistivity result at site 105 is shown as a dash line.

LAYERED MODELS OFF THE GRANITE

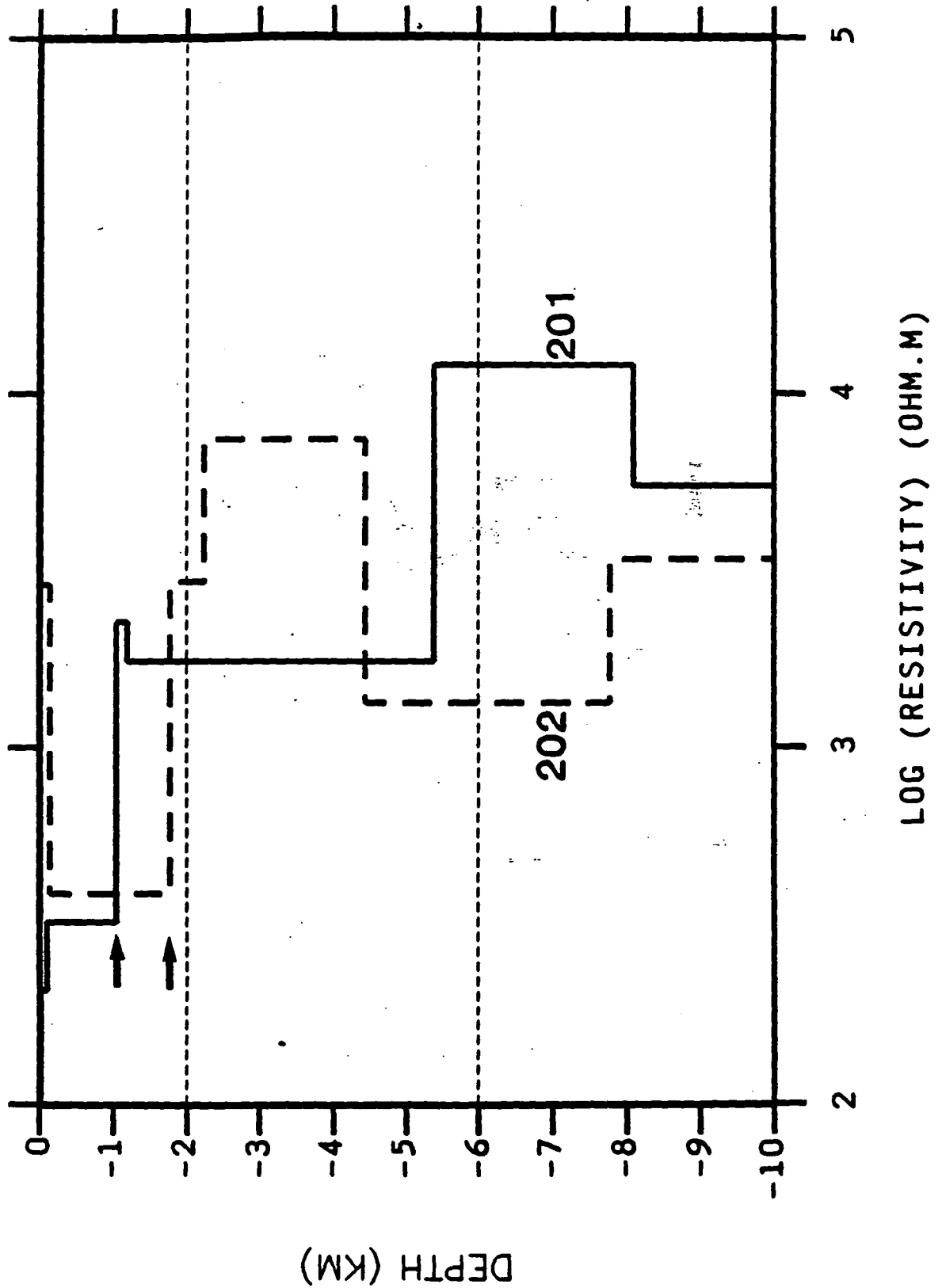


Figure 9. 1-D inversion results (layered models) for the two SET 2 off-granite sites. The data possess 2-D (site 201) and 3-D (site 202) characteristics. The transition depths to resistivities greater than 1000 ohm.m are arrowed.

SMOOTH MODELS ACROSS THE GRANITE

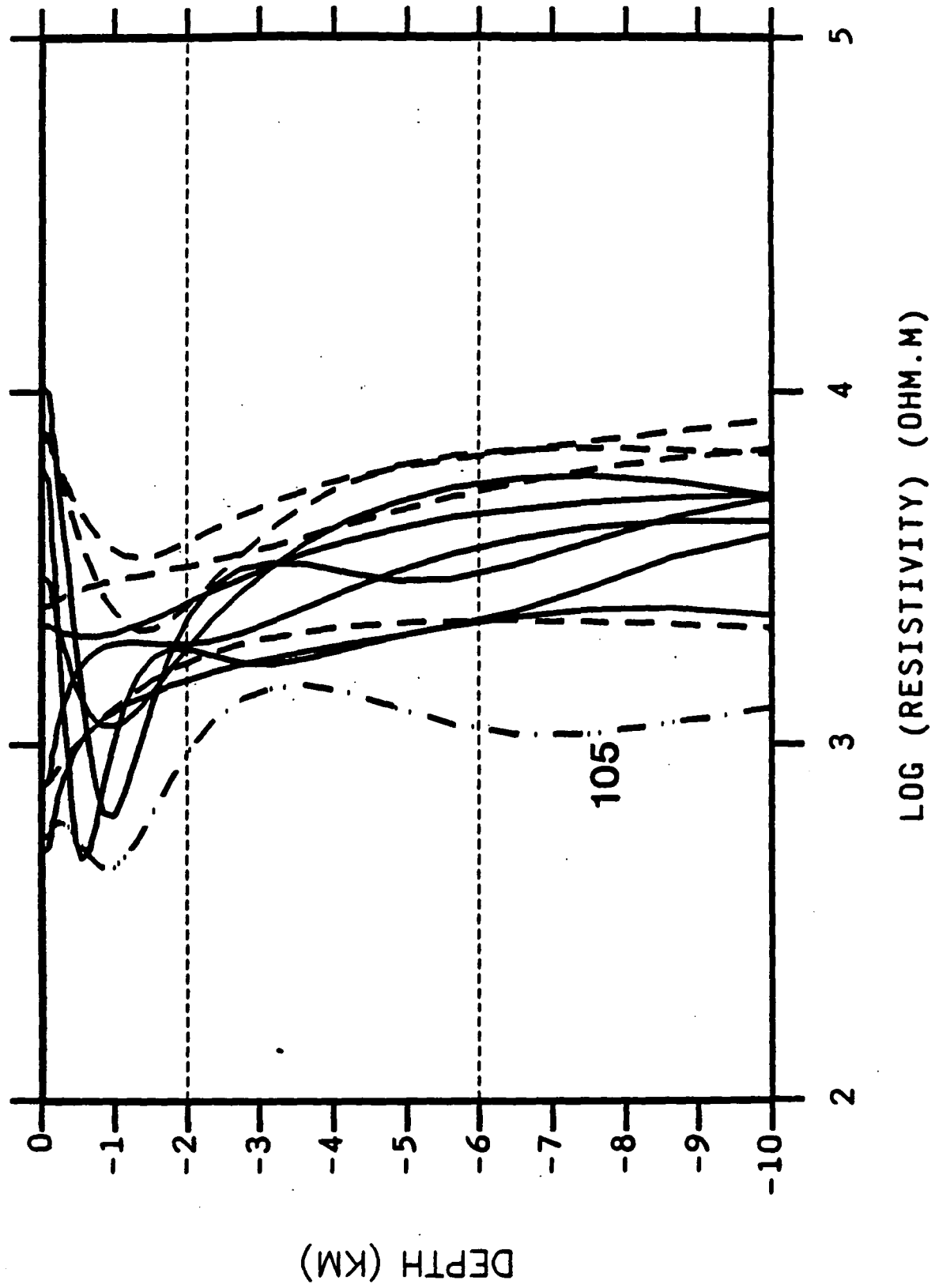


Figure 10. 1-D inversion results (smooth models) for the SET 1 profile sites. The lower resistivity result at site 105 is shown as a dot-dash curve. The eastern-most sites (109-112) are shown as dash curves.

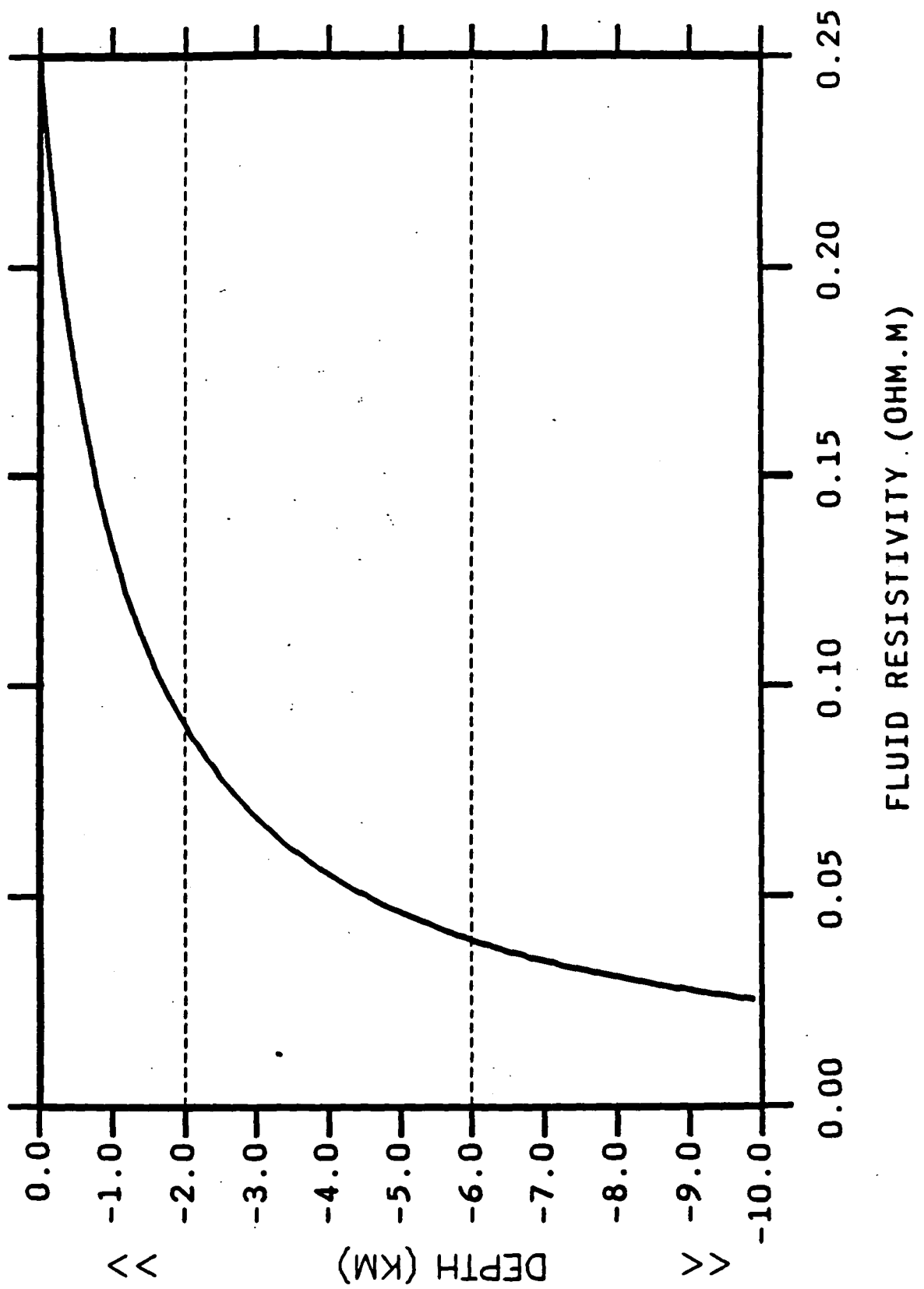


Figure 11. Variation of fluid-resistivity with depth calculated from the temperature dependent variation and using the predicted temperature-depth profile of the Carnmenellis granite (Fig. 2).

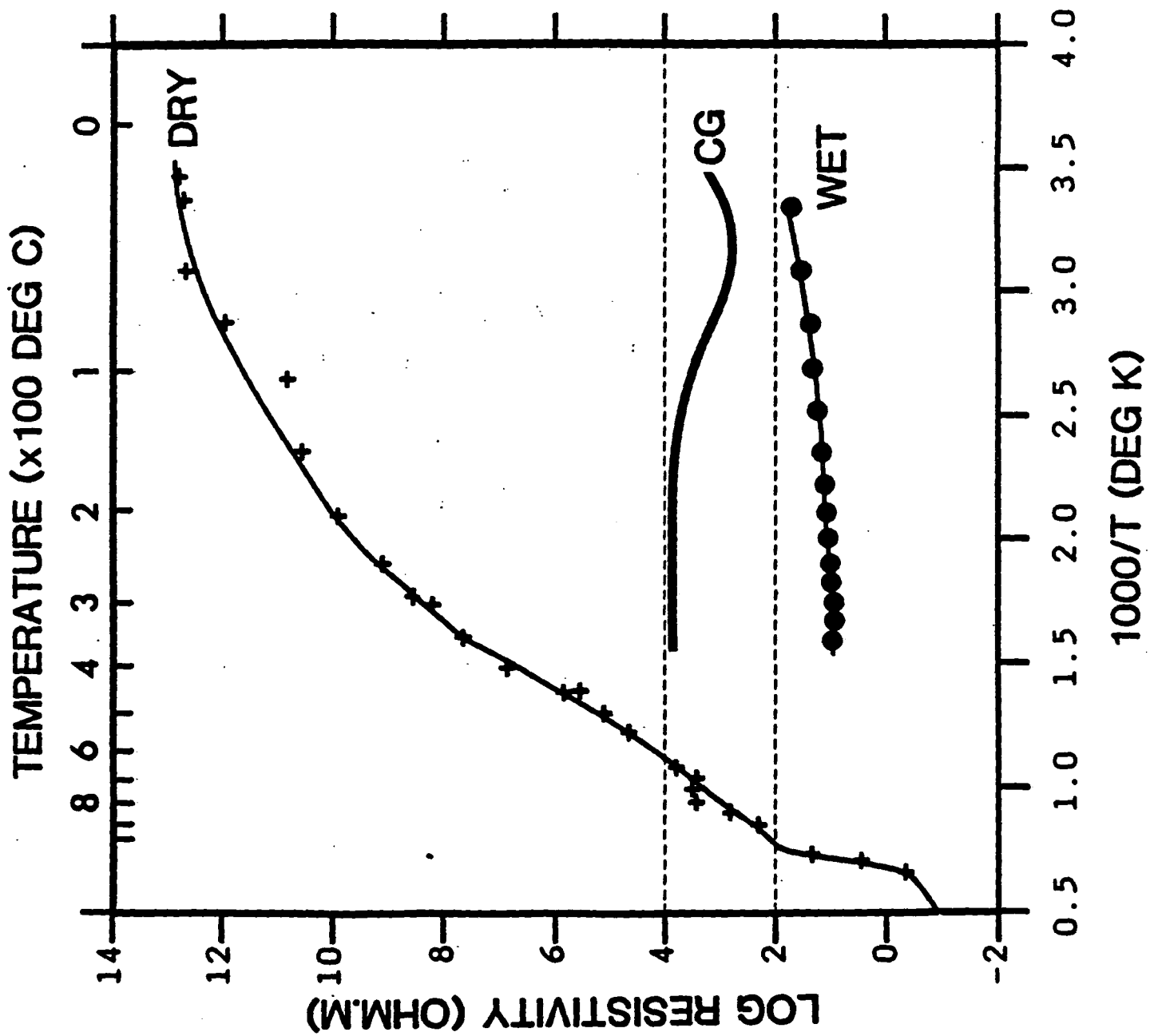


Figure 12. Summary of the laboratory data on the variation of resistivity with temperature for wet and dry granite (after Olhoeft 1981). Crosses (dry curve) are vacuum dry (10^{-11} MPa) Westerly granite. Closed circles (wet curve) are 0.4 molar NaCl solution-saturated Westerly granite. A representative resistivity curve for the Carmenellis granite (CG) is also shown.

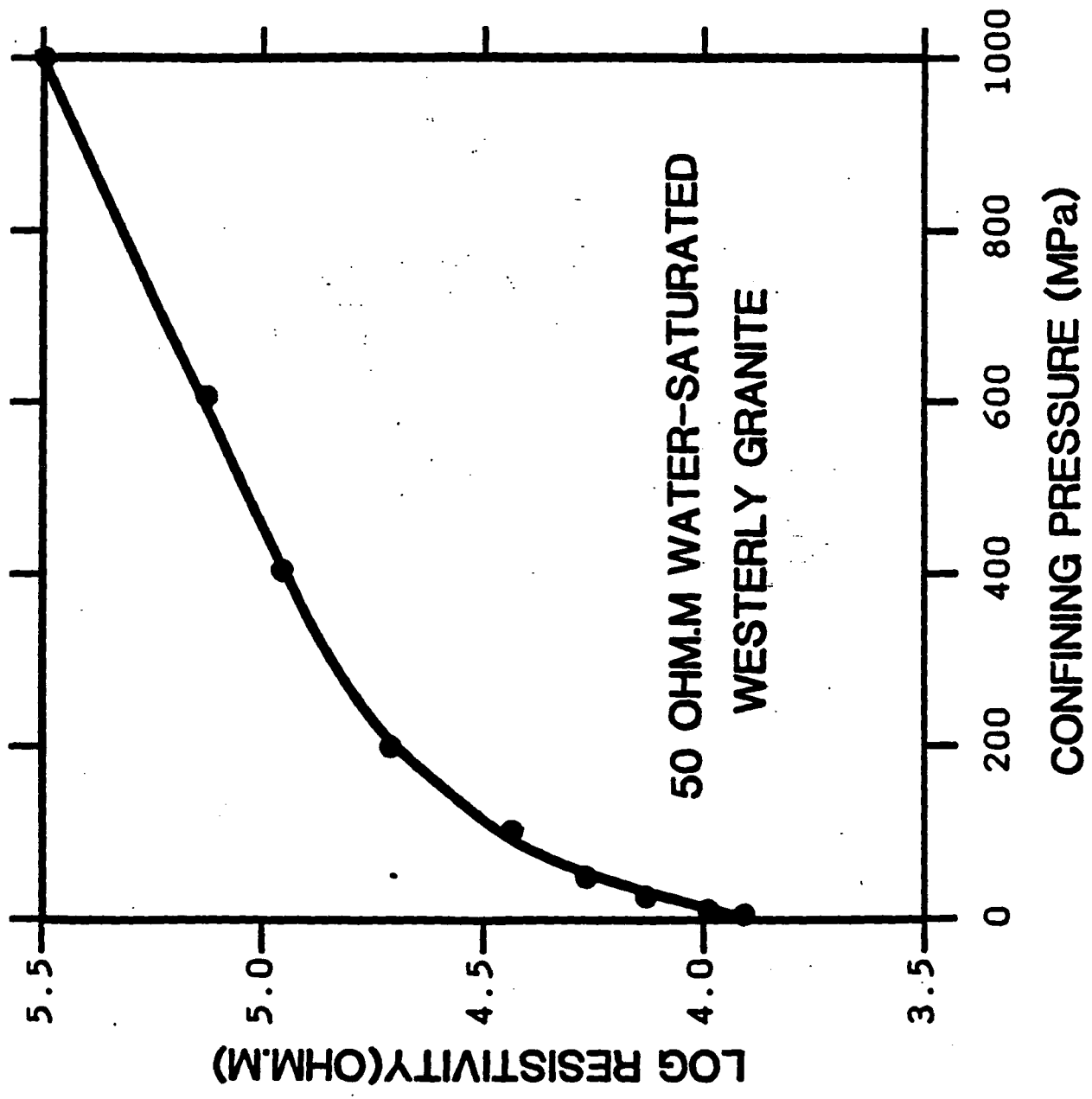
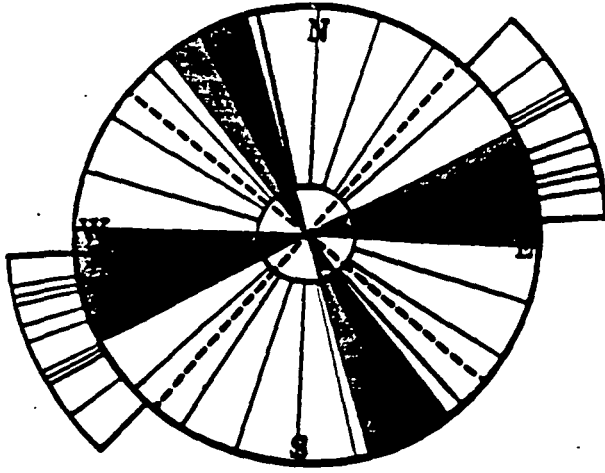
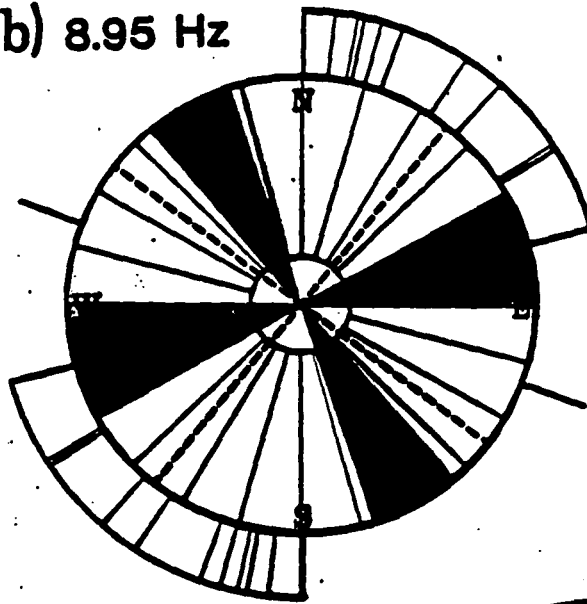


Figure 13. The effect of confining pressure on water-saturated Westerly granite (after Brace and Orange 1968b and Olhoeft 1981). The curve is considered typical of all fluid-saturated crystalline rocks.

(a) 89.5 Hz



(b) 8.95 Hz



(c) 0.089 Hz

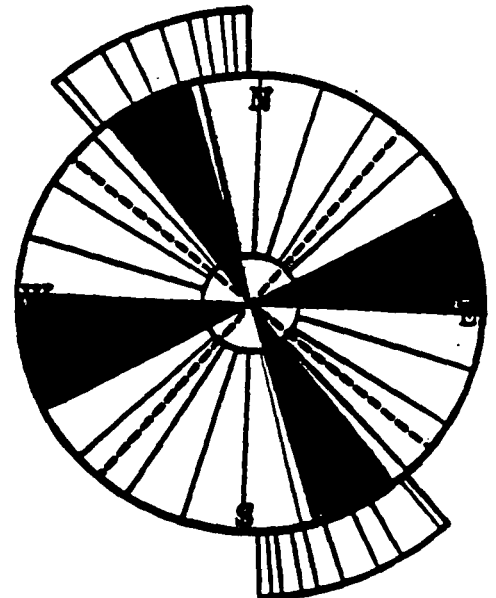


Figure 14. A comparison of the joint and stress directions with the azimuths of maximum resistivity for the SET 1 profile sites at three frequencies (penetration depths). The inner full-circle derives from Fig. 3 and shows joint sets (shaded) and stress directions (dotted). The outer (segment) azimuths contain the azimuths of maximum resistivity observed at individual locations across the granite.